The effect of antimicrobial peptide indolicidin and its analogues on human embryonic stem cells

Lasse Hyldgaard Klausen

M.Sc Thesis

AAU, 2011-2012

AALBORG UNIVERSITY

THE UNIVERSITY OF EDINBURGH

AALBORG UNIVERSITY

Department of Physics and Nanotechnology
Skjernvej 4A
DK-9220 Aalborg
Phone 9940 9215
Fax 9815 6502
http://www.nano.aau.dk/

Title:	The effect of antimicrobial peptide indolicidin and its analogues on human embryonic stem cells.
Project period:	September 2011 - June 2012
Author:	Lasse Hyldgaard Klausen
Supervisor:	Leonid Gurevich
Copies:	4
Number of pages:	100
Number of appendices:	4
Project finished:	June, 2012

Synopsis

Human embryonic stem cell research is a rapidly evolving field with a great potential. Embryonic stem cells can continuously reproduce themselves, and they are capable of forming the entire diversity of cells in an adult. The growth of these cells *in vitro* requires a high level of control and the culture systems are constantly improving. Embryonic stem cells are distinct from other cells in many aspects, and the presence of the DNA base 5-hydroxymethylcytosine was recently found - a DNA base that in mammalian cells is almost exclusive to embryonic stem cells.
Indolicidin is an antimicrobial peptide with a unique DNA binding capacity that can inhibit the DNA synthesis in bacteria. The effect of binding to mammalian DNA has not yet been properly investigated, and the possibility of an effect from binding to 5-hydroxymethylcytosine in embryonic stem cells was the initial idea for this project.

The effect of indolicidin, the analogue indolicidin-4 and a new peptide IL4-RWT was tested on the embryonic stem cell lines RH1 and T8. The cells were maintained in a culture system of Matrigel™ and mTeSR®1. Cytotoxic concentrations were determined, and IL4-RWT, that contains the fluorophore rhodamine WT, was used to test the cellular uptake of the peptide. Flow cytometry showed a slow linear uptake indicating an endocytosis related pathway and this was confirmed by fluorescence confocal laser scanning microscopy showing inclusion bodies.

The effect of IL4 on the pluripotency of RH1 cells was first tested using a short assay. The morphology of the cells was monitored and the expression of pluripotency transcription factors Oct-4 and Nanog was determined using real-time reverse-transcription PCR. No significant effect was observed and a longer assay using the T8 cells was conducted with IL and IL4. A clear positive effect was observed for IL4, but a karyotype test revealed a mosaic making the results void.

DNA was isolated from the adult HDF cells and from the RH1 cells. The DNA was fragmented using ultrasonication or digestion and imaged using AFM. Ultrasonication provided DNA of the desired size without the need for extra cleanup steps as with enzymatic digestion, and this method was used to prepare DNA for testing with IL4. The binding of IL4 to both HDF and RH1 DNA was confirmed, and a fast and easy method for visualisation and analysis of the DNA molecules was described.

Resume

Forskning i menneske embryoniske stamceller er et hastigt udviklende område med et stort potentiale. Embryoniske stamceller kan ubegrænset reproducere sig selv, og de er i stand til at danne hele mangfoldighed af celler i en voksen krop. Væksten af disse celler *in vitro* kræver en høj grad af kontrol og kultur systemerne bliver konstant forbedret. Stamceller adskiller sig fra andre celler i mange henseender, og tilstedeværelsen af DNA basen 5-hydroxymethylcytosin blev for nylig fundet; en DNA-base, der i mammale celler næsten kun findes i embryoniske stamceller.
Indolicidin er et antimikrobielt peptid med en unik DNA-interagerende egenskab, der kan inhibere DNA-syntese i bakterier. Virkningen af binding til mammal DNA er endnu ikke er blevet tilstrækkeligt undersøgt, og muligheden for en interaktion med 5-hydroxymethylcytosin i embryoniske stamceller var den indledende ide til dette projekt.

Virkningen af indolicidin, analogen indolicidin-4 og det nye peptid IL4-RWT blev testet på de embryoniske stamcelle linjer RH1 og T8. Cellerne blev groet i et kultur system af Matrigel^{TM} og mTESR ®1. Cytotoksiske koncentrationer blev bestemt, og IL4-RWT, der indeholder fluorophoren rhodamin WT, blev anvendt til at teste cellulær optagelse af peptidet. Flowcytometri viste en langsom lineær optagelse, hvilket indikerer en endocytose relateret pathway og dette blev bekræftet med fluorescens konfokal laserscanningsmikroskopi, der vidste inklusionslegemer.

Virkningen af IL4 på pluripotensen af RH1 celler blev først testet ved anvendelse af et kort assay. Morfologien af cellerne blev overvåget, og udtrykningen af pluripotens transkriptionsfaktorer Oct-4 og Nanog blev bestemt ved anvendelse af real-tids revers transkriptase PCR. Ingen betydelig virkning blev observeret, og en længere analyse af T8 celler blev udført med IL og IL4. En klar positiv effekt blev observeret for IL4, men en karyotype test afslørede en mosaik, der gjorde resultaterne ubrugelige.

DNA blev isoleret fra de voksne HDF celler og fra RH1 celler. DNA'et blev fragmenteret med ultralydbehandling eller med restriction enzymer og scannet med AFM. Ultralydbehandlingen producerede DNA med den ønskede størrelse uden behov for ekstra oprensningstrin som med enzymatisk nedbrydning, og denne fremgangsmåde blev anvendt til klargøringen af DNA til test med IL4. Bindingen af IL4 til både HDF og RH1 DNA blev bekræftet, og en hurtig og nem fremgangsmåde til visualisering og analyse af DNA molekyler blev beskrevet.

Preface

This report was made as part of the 9th and 10th semester of Nanobiotechnology at the Department of Physics and Nanotechnology, Aalborg University. First part of the project was conducted from 1st of September 2011 to 24th of February 2012 with the group of Dr. Paul A De Sousa at the MRC Centre for Regenerative Medicine, Edinburg University. Second part of the project was conducted from 27th of February 2012 to 15th of June 2012 at the the Department of Physics and Nanotechnology, Aalborg University.

The report includes five chapters and 4 appendices. Citations are done using a number method, where a bracket contains a number connected to the source position in the reference section. In the text, a reference that is placed before a full stop refers to that specific sentence. References that are placed after a full stop refers to the previous subsection.

Figures and tables are numbered in accordance to the section and order of appearance. References are made using the abbreviations Figure, Table, Section and Appendix respectively. If there is no citation in the caption of the figure, it has been produced by the author.

I would like to thank *Dr. Paul A De Sousa* for giving me the unique opportunity of working with his group, help in planning the project and an overall warm welcome. I would also like to thank the members of Edinburgh University *Dr. Steve Pells*, *Dr. Marieke Hoeve* and *Dr. Nina G Bauer* for aid in planning of experiments, *Heidi Mjoseng* for introduction to embryonic stem cell maintenace, *Eirini Koutsouraki* for introduction to qPCR, *Kay Samuel* for help conducting fluorescence activated cell sorting and *Martin Stindl* for aid in manual SPPS.

Abbreviations

AFM	Atomic force microscopy
AMP	Antimicrobial peptide
bp	Base pairs
DCM	Dichloromethane
DMF	Dimethylformamide
DNA	Deoxyribonucleic acid
E. coli	*Escherichia coli*
EGFP	Enhanced green fluorescent protein
Fmoc	9-fluorenylmethyloxycarbonyl
GABA	γ-aminobutyric acid
HDF	Human dermal fibroblast
hESC	Human embryonic stem cells
ICM	Inner cell mass
IL	Indolicidin
IL4	Indolicidin-4
IL4-RWT	Indolicidin-4 + rhodamine water tracer
kbp	Kilo base pairs
LiCl	Lithium Chloride
MeOH	Methanol
Oct-4	Octamer-binding transcription factor 4
PA	Pipecolic acid
PBS	Phosphate buffered saline
RH1	Roslin Human 1
RP-HPLC	Reverse-phase high performance liquid chromatography
TFA	Trifluoroacetic acid
TGF-β	Human transforming growth factor β
TIS	Triisopropylsilane
5-mC	5-methylcytosine
5-hmC	5-hydroxymethylcytosine

Contents

1 Introduction

Stem cells are a unique subset of cells that play a crucial role in the development and regeneration of human life. They are important cells defined by the ability to continuously reproduce themselves, but meanwhile retaining the ability to differentiate into various cell types. These characteristics make stem cells ideal candidates for cell therapy or tissue engineering applications, and the use of stem cells in regenerative medicine is a both promising and rapidly growing field[1]. Stem cells are found at all developmental stages, from embryonic stem cells - capable of forming the entire diversity of cells in the adult organism - to adult stem cells, identified in most tissue types responsible for maintenance and repair of the surrounding tissue[2]. Adult stem cells have been used in medicine for more than 50 years in applications such as bone marrow infusion for leukemia treatment[3]. The use of embryonic stem cells on the other hand is an emerging field often limited by ethical controversies, but limitations of adult stem cells makes the future development imperative: Most adult stem cells have a limited lifespan in culture and they typically generate only the cell types of the tissue in which they reside[4], while embryonic stem cells have full developmental potential to differentiate into any type of cell or tissue in the body, and they have an almost unlimited self-renewal capacity in culture[2].

Controlling the growth and differentiation of embryonic stem cells is however a complex process. The cells require specialised media and substrate conditions, and specialised feeder cells are often used just to keep the cells from differentiation[5]. Embryonic stem cells are normally controlled by the use of a specialised extracellular matrix and the addition of cytokines and growth factors that all target pathways associated with the differentiation, survival and proliferation of the cells. Delivery of proteins into the cell, instead of targeting surface receptors, provides a more direct approach. An example of the use of intracellular targeting proteins was the use of a poly-arginine sequence to transport reprogramming factors into somatic cells creating induced pluripotent stem cells, adult cells reprogrammed to an ESC-like state[6].

Indolicidin is an antimicrobial peptide[7] that has been demonstrated to interact with DNA in bacteria preventing proper cell division[8]. The DNA binding affinity of indolicidin and analogues have been intensely investigated[9,10,11,12,13], but the effect of binding to mammalian DNA has not yet been explored. Mammalian DNA differs from prokaryotic DNA in certain aspects, such as the packaging in the chromatin, residency in the cell nucleus and the amount of chemical modifications. The binding of indolicidin to mammalian DNA might therefore have a different effect than observed in bacteria. The DNA base 5-hydroxymethylcytosine is in mammalian cells almost exclusive to embryonic stem cells,

bone marrow and brain[14], and this DNA modification might also influence the outcome of indolicidin binding to DNA. A membrane penetrating ability combined with a unique interaction with DNA makes indolicidin a possible instrument in the control of embryonic stem cells.

1.1 Human Embryonic Stem Cells

The initial stem cell is the fertilised egg formed through the joining of male and female gametes. The oocyte (unfertilized egg) and spermatocyte are formed during the first part of meiosis and both contain only half the number of chromosomes found in normal somatic cells. During the second part of meiosis the two fuse and the zygote is formed with a genotype comprising half maternal and half paternal chromosomes. The zygote is totipotent, meaning that it is able to produce all differentiated cell types. The first cell divisions (mitosis) of the zygote are called cleavage and the formed cells are called blastomers. The blastomers become increasingly smaller, but up to the 8-cell stage they are considered as totipotent. As the number of blastomers approaches 32 to 64 cells, a sphere of cells, the blastocyst, is formed with an inner cell mass (ICM) later forming the embryo and outer cells later forming the embryonic membranes and placenta. Human embryonic stem cell (hESC) lines are derived from the inner cell mass of the blastocyst and as such are pluripotent, and they can under appropriate conditions undergo differentiation to give rise to any cell type in the body.[15,2]

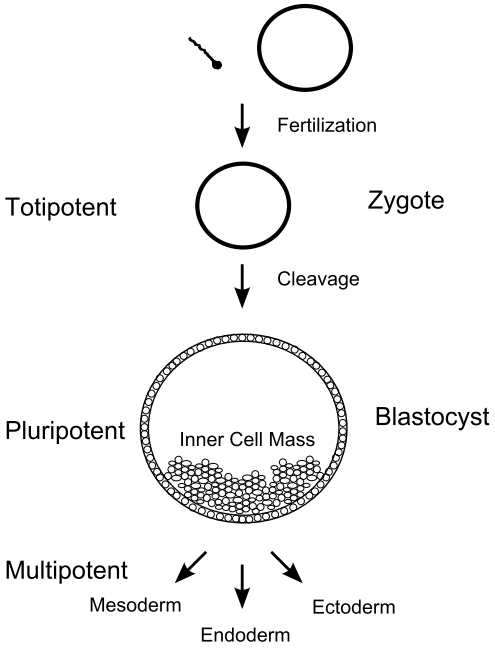

Figure 1.1: *Early development of embryo. The joining of male and female gametes creates the totipotent zygote. The zygote divides during cleavage and eventually loses totipotency as the blastocyst is created. The inner cell mass (ICM) of the blastocyst is isolated and cultivated creating pluripotent embryonic stem cells. The pluripotent cells can form all three of the germ layers.*

Once isolated from the blastocyst, the hES cell line is propagate in an environment that allows for cell growth, but at the same time prevents the cells from differentiating. Such environment traditionally con-

sist of a layer of mitotically inactivated fibroblast, called feeder cells, but feeder-free conditions have also been applied[16,17]. Quality control, or selection of ES cells from differentiated cells when need be, is done using the specific properties of the cell line. ES cells have an almost unlimited self-renewal capacity and as such are not subjected to the cellular aging of somatic cells related to telomere shortening. The telomere is a region of repetitive nucleotide sequences at the end of a chromosome, which is shortened through each cell division until it reaches a certain size, known as the Hayflick Limit, where cell division stops. Immortal cells overcome the Hayflick Limit by expression of telomerase, an enzyme responsible for maintaining telomere length. A high level of telomerase activity in ES cells compared to somatic cells can be expected[18]. ES cells are also characterised by a high alkaline phosphatase activity[16], expression of the transcription factor Oct-4, which is exclusive to blastomeres, pluripotent early embryo cells and the germ cell lineage[19]. Certain surface markers such as SSEA–3, SSEA-4, TRA-l-60 and TRA-1-81, which were all used in the first establishment of human embryonic stem cells[16], and transcription factors such as Oct4, Sox2, c-myc, Klf4, Nanog or Lin28, used in the first reprogramming of adult stem cells to pluripotent stem cells[20,21], also characterise pluripotent hES cells.

The morphology of ES cells versus differentiated stem cell is often evident, where pluripotent cells appear as compact cells in well defined colonies and with a high nuclear to cytoplasmic ratio, while differentiated cells tend be more dispersed and display a flatter morphology[22].

The T8 hES cell line

The T8 cell line is a tranfected human embryonic stem clonal cell line. H1[16] cells were transfected with an Oct4-EGFP plasmid, which express enhanced green fluorescent protein under control of the Oct4 promoter. If Oct-4 expression is downregulated upon differentiation, the EGFP signal becomes a reporter of pluripotency. A G418 resistance marker is also incorporated under control of the Oct-4 promoter. The T8 cell line is of normal XY human karyotype.[23,24]

The RH1 hES cell

The Roslin Human 1 human embryonic stem cell line was after isolation propagated on a humanised media using human dermal fibroblast as substitution for the earlier use of mouse embryonic fibroblast. The cell line is XX euploid and carries a pericentric inversion of chromosome 9, which is considered to be a normal human karyotype variant[17].

1.1.1 Human Embryonic Stem Cell Growth Conditions

Propagation of hES cells in culture must be done with an optimal growth rate and without the loss of differentiation potential. This is traditionally done using mouse embryonic fibroblast feeder cell layers, but the use of feeder cells includes risks. Mouse feeder cells can sustain both mouse and human ES

cells, but the specific factors currently identified that sustain mouse ES cells do not support human ES cells[25], and the excess of conditioning factors provided by the feeder cells may have unwanted effects. Evidence of such can be provided by the influence of either mouse feeder cells or bovine derived "serum replacement", which was the cause of human ES cells suddenly expressing a non-human sialic acid, rendering the cells unsuitable for medical use[26]. Replacing animal feeder cells and animal derived serum with human constituents removes the risks of zoonosis, but the use of serum products can give batch variations[27,28]. The ideal environment for controlled ES cell growth is chemically defined and such cell culture systems have been described[28], but the cost of some defined components often make them impractical for everyday use. The main system used in this project is the media mTESR®1, which includes bovine serum albumin (BSA)[25], and the support Matrigel™, a complex mixture of matrix proteins derived from Engelbreth-Holm-Swarm mouse tumors[29].

1.2 Epigenetics of Embryonic Stem Cells

Epigenetic mechanisms refer to heritable changes in the gene expression of a cell other than changes in the DNA sequence. The epigenetic state of a cell is inherited and can continue as "memory" of a cell through many cell divisions[30], and it is in the epigenetic state that the difference between cell types of identical DNA sequences lie. The pluripotent state of embryonic stem cells is the result of specific epigenetic processes that regulate the expression of genes in regulatory and coding regions[31].

Epigenetic mechanisms include modifications of the nucleotides and the proteins in the chromatin. The main type of nucleotide modification is the conversion of cytosine to 5-methylcytosine (5-mC), also known as DNA methylation. DNA methylation usually happens on CpG dinucleotides (cytosine followed by guanine), and 70%–80% of all CpG dinucleotides in human somatic cells are methylated[32]. Dense clusters of CpGs are know as "CpG islands", they are often found in promoter regions and it has been observed that methylation of the CpG island is inversely correlated with gene expression[33]. Embryonic stem cells possess a unique methylation signature compared to differentiated cells and cancer cells[34], and pluripotent cells have been shown to possess a slightly higher overall methylation level of CpG dinucleotides than fibroblast cells[35]. Methylation of cytosine in a non-CpG context is most common in embryonic stem cells with nearly one-quarter of all methylation in non-CpG dinucleotides. Non-CpG methylation is reduced upon induced differentiation[36].

1.2.1 5-Hydroxymethylcytosine in Embryonic Stem Cells

5-Hydroxymethylcytosine (5-hmC) is a DNA base first identified in 1953 in the bacteriophage T2, T4 and T6[37]. The presence of 5-hmC in mammalian cells was indicated in 1972[38], but only few mentions

were made till recently when the base in 2009 was identified in mammalian cells[39,40] and in particular in mouse embryonic stem cells. An analysis of MspI cleavage sites in mouse embryonic stem cells showed 4% of all cytosine species in CpG dinucleotides to be hydroxymethylated equaling 0.1% of all cytosines in the genome[39]. 5-hmC may not be confined to CpG as is the case with 5-mC, and the total percentage of 5-hmC is possible higher.

5-Hydroxymethylcytosines in DNA bacteriophages are glycosylated as part of a protective strategy towards bacterial restriction enzymes[41], while the use of the base in mammalian cells is most likely connected to a demethylation process catalysed by the Tet proteins[42].

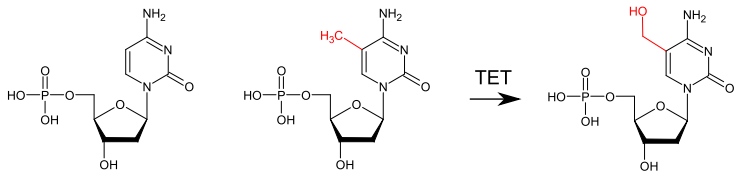

Figure 1.2: *Epigenetic modifications of the cytosine DNA base. Methylation of the 5 position of the cytosine pyrimidine ring (5-mC) is often found in CpG dinucleotides, where methylation in promoter regions is inversely correlated with gene expression. 5-Hydroxymethylcytosine is formed by hydroxylation of 5-mC by Tet proteins and may be part of a demethylation process important for embryonic stem cells.*

1.3 The Antimicrobial Peptide Indolicidin

Antimicrobial peptides are host defence molecules produced by the innate immune system of species throughout the animal and plant kingdom. The diversity of antimicrobial peptides is even greater than the diversity of species from which they have been discovered, and the same peptide sequence is rarely recovered from two different species[43]. The general features of antimicrobial peptides is a cationic charge, a length of about 12-50 amino acids and some degree of amphipathicity due to a content of both hydrophilic and hydrophobic amino acids[44]. Four main structural classes of antimicribial peptides are normally considered based on their secondary structure. The four structural classes are: β -sheet molecules stabilised by two or three disulphide bonds, amphipathic α -helices, extended molecules, and loop structures created by a single disulphide bond[45]. Indolicidin does not exhibit either α or β structures and belong to the class of extended molecules[46].

Indolicidin is a 13 residue long cationic peptide isolated from the cytoplasmic granules of bovine neutrophils[8]. It has the amino acid sequence ILPWKWPWWPWRR-NH2, from which it is seen that indolicidin contains both hydrophilic and hydrophobic amino acids and carries a net charge of +4 including terminal amidation. It is characterised as a Trp-rich peptide owing to the five tryptophan residues. The high degree of proline residues may contribute to why indolicidin does not adopt either α-helical or β-sheet conformation, not even in membrane mimicking environments. However, it is well established

that indolicidin readily partitions itself into membrane bilayers of different lipid compositions, adopting an extended wedge-like conformation.[47,8]

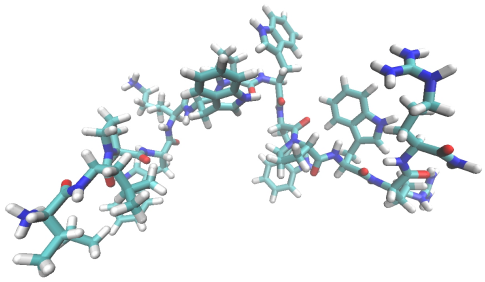

Figure 1.3: *NMR determined structure of indolicidin bound to dodecylphosphocholine micelles[46]. Adapted from entry 1G89 of the RCSB Protein Data Bank.*

Indolicidin has been shown to possess significant antimicrobial effects against Gram-positive and Gram-negative bacteria, fungi and protozoa[9], and has furthermore been shown to have the ability to inactivate HIV-1[48]. All these abilities can be explained by the hypothesis that indolicidin has a membrane disrupting property, which however has not yet been fully understood[49]. Several different ideas about the mode of action of indolicidin exist. Falla *et al.*[50] reports that the killing mechanism involves a barrel-stave pore formation, whereas Shai *et al.*[51] suggest the toroidal model as the mode for indolicidin to cross the membrane. Yet again, others suggest that the mechanism is without well defined pore formation, and that the uptakes is caused by some sort of membrane aggregate that allows indolicidin to penetrate into the cytoplasm[52]. Even though the mechanism is still inconclusive, Subbalakshmi *et al.* confirms that indolicidin has the ability to permeabilise the inner and outer layers of bacterial membranes without lysing the cells[8].

Indolicidin induces filamentation in *E. coli* at concentrations below the required for lysis of the bacterial membrane. This happens as a result of indolicidin binding to DNA, inhibiting DNA synthesis but otherwise not significantly affecting either RNA or protein levels[8]. The DNA binding affinity and unique tryptophan and proline content of indolicidin has attracted a lot of attention and brought about a considerable amount of structural analogs.

1.3.1 Indolicidin Analogs

The short nature of indolicidin combined with the high proportion of tryptophan (38%) and proline (23%) residues is believed to be involved in the antibiotic effect, but it also causes indolicidin to have a cytotoxic nature, which impairs its therapeutic use[53]. Many indolicidin derivatives have been created, testing the effect of etc. tryptophan[50] and proline[54] in order to minimise the hemolytic activity, while retaining the antimicrobial effect. The indolicidin analogue omiganan (ILRWPWWPWRRK-NH_2)[55] has even

passed phase III trials and demonstrated statistically significant bactericidal and fungicidal effect[56].

Indolicidin analogues with tryptophan replaced by phenylalanine[57] or leucine[50] has been produced, and a decreased hemolytic activity has been observed. The replacement of 4 tryptophan with leucine produced the indolicidin analogues IL-4, IL-8 and IL-11, where the number indicates the last remaining tryptophan. Earlier studies on IL4 using high-resolution AFM imaging has indicated an affinity for the double helix structure of DNA comparable to that of indolicidin.

1.4 Atomic Force Microscopy

Atomic force microscopy (AFM) is a class of scanning probe microscopy (SPM), where a physical probe is mechanically moved over a sample, generating an image by measuring the interaction between probe and surface[58]. AFM measures the force and at short separation the force between neutral atoms or molecules can be described by the Lennard-Jones potential:

$$w(r) = \varepsilon \left[\left(\frac{r_e}{r} \right)^{12} - 2 \left(\frac{r_e}{r} \right)^{6} \right] \tag{1.1}$$

where ε is the potential well depth, r is the separation between two particles and r_e is the separation at equilibrium. The Lennard-Jones potential is plotted in Figure 1.4. Force is the negative slope of potential and an attractive force occurs between particles at separation larger than r_e due to Van der Waals interactions $[(r_e/r)^6]$, while a repulsive force occurs at separation smaller than r_e due to Pauli repulsion $[(r_e/r)^{12}]$.[59]

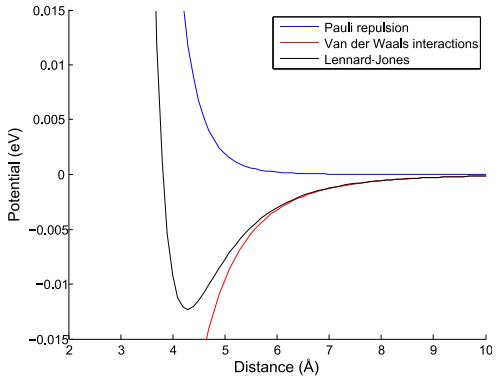

Figure 1.4: *The Lennard-Jones potential plotted as function of separation. ε and r_e values for methane empirically determined[60]. Plotted in MATLAB.*

The ultimate resolution of AFM is critically defined by the radius of the AFM tip. A single atom tip would theoretically give an optimal resolution, but such a tip is also very fragile. Once the tip touches the sample surface, no matter how soft the contact or gentle the touch, the tip will instantly become blunt. Non-Contact mode AFM involves the use of an oscillating cantilever moving slightly above the sample.

The tip is oscillated close enough to the surface that the Van der Waals forces between tip and surface will affect the resonance frequency and amplitude of the cantilever. The impact is then used to maintain the tip-sample separation constant so that a high resolution profiling of the surface can be obtained.[61]

A liquid meniscus layer will form on most samples in ambient conditions. In non-contact mode AFM the tip is oscillated with a small amplitude (< 5 nm) near the surface, and there is only a narrow region where the oscillation amplitude is affected by the Van der Waals interaction, before the tip is captured by the surface liquid. Once the tip is captured, a force is required to pull out the tip and resume a free oscillation. To overcome this problem a larger amplitude is applied (typically 20-100 nm). The tip now "taps" the surface, thus overcoming the stickiness of the liquid layer. This method is referred to as tapping mode.[62]

A simplified setup of an AFM is shown in Figure 1.5. A laser signal is reflected from the top of a cantilever to a photodiode array, and the angle of reflection is used to measure the z-position of the tip. The layout amplifies small changes in height of the cantilever and enables measurement of picometer resolution[58]. Figure 1.5 B illustrates a tip scanning a surface. A single atom tip is not practical and the effect of tip curvature on the lateral resolution is evident. AFM can therefore only provide precise quantitative information about the height of a structure and not the width.

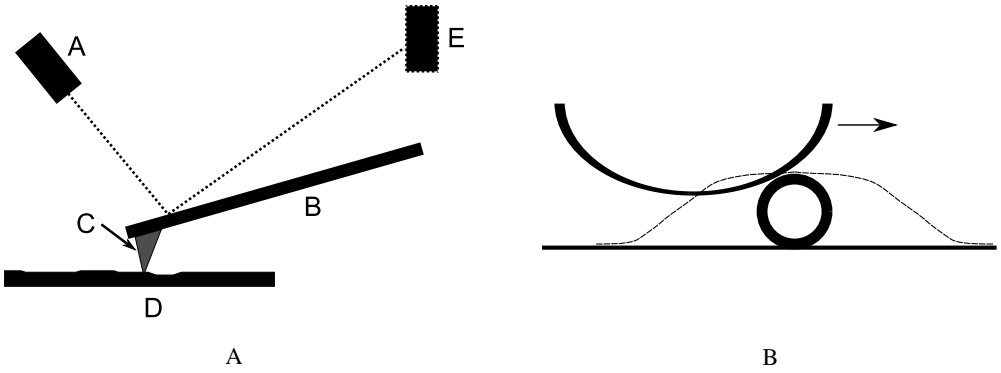

Figure 1.5: *Atomic force microscopy. A: Scheme of an AFM setup with laser (A), cantilever (B), tip (C), sample (D) and photodiode array (E). B: The effect of tip curvature on lateral resolution.*

1.5 Structure of DNA

DNA is a nucleic acid containing the genetic material of the cell. DNA is found in all living organisms (excluding viruses as non-living) with little difference in the molecular structure. The DNA molecule is a long polymer composed of the four nucleotides adenine (A), thymine (T), cytosine (C) and guanine (G). The nucleotides are composed of a base, 2-deoxyribose and a phosphate group, where the phosphate and 2-deoxyribose link the nucleotides forming a strand. The DNA molecule consists of two helical strands coiled around the same axis held together by hydrogen bonds formed between the bases facing

each other. Pairing of the bases obey the complementary base pairing principle stating that adenine pairs with thymine forming two hydrogen bonds, while guanine pairs with cytosine through three hydrogen bonds. The structure of the four bases is shown in Figure 1.6 (A). Figure 1.6 (B) shows the double-helical B-form of the two DNA strands as determined by Watson and Crick.[63]

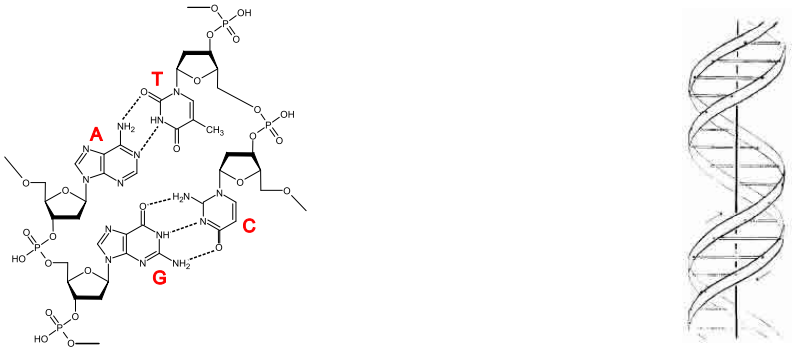

Figure 1.6: *The structure of DNA. A: The four nucleotides adenine (A), thymine (T), cytosine (C) and guanine (G) that make up the DNA molecule. B: The double-helical structure of DNA as first published by Watson and Crick in 1952*[63].

The helical structure of the DNA molecule displays a great deal of plasticity. The B conformation of DNA is believed to be predominant in cells, but other conformations such as the A and Z also exist. The conformation that DNA adopts depends on the hydration level, supercoiling, chemical modifications of the bases, concentration of ions and the DNA sequence[64]. The A, B and Z conformations are the most common and the direction of the helix, residues per turn and diameter in solution are listed in Table 1.1. Non-canonical DNA structures also exist, such as parallel helices[65], Holliday junctions[66] or G-quadruplexes that hold important biological functions[67].

	A-DNA	**B-DNA**	**Z-DNA**
Helix sense	Right	Right	Left
Residue per turn	11	10-10.5	12
Axial rise (Å)	2.55	3.4	3.7
Diameter (Å)	23	20	18

Table 1.1: *Selected geometric properties of A, B and Z conformation of DNA.*[68]

The molecular structure of DNA so far described is valid for both pro- and eukaryotic cells. The general layout of eukaryotic cells is shown in Figure 1.7. Both plant and animal cells are surrounded by a lipid bilayer that confines the cytoplasm. Inside the cytoplasm a variety of organelles exist, usually enclosed by independent membranes. The nucleus is a special organelle that holds the DNA of eukaryotic cells. The membrane of the nucleus is selectively permeable and allows certain material such as mRNA to move between the nucleus and cytoplasm, while DNA is confined to the nucleus[69]. Most molecules smaller than 10 nm in diameter can normally diffuse freely through the nuclear membrane, while larger molecules require a specific amino acid motif for translocation[70]. Other organelles in eukaryotic cells also contain DNA, such as the chloroplast in many plant cells and mitochondria in animal cells. Human

cells contain approximately 100-10,000 copies of the mitochondrial DNA, each of approximately 16,000 base pairs[71], which is a fairly small proportion of the total cell DNA.

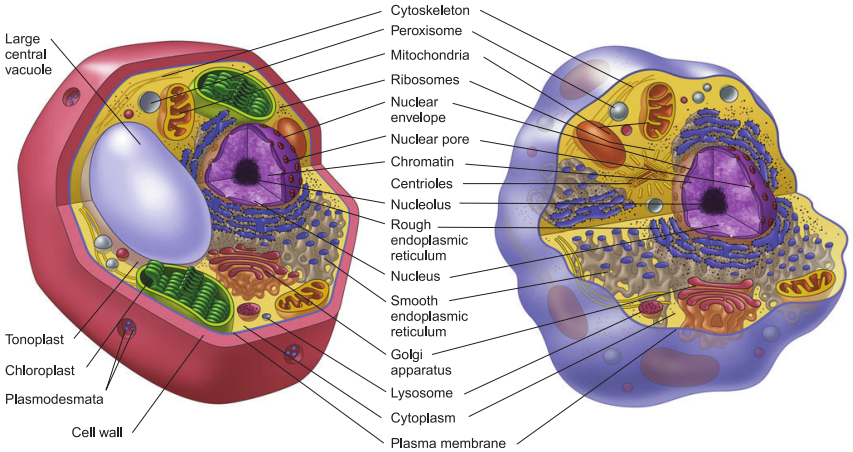

Figure 1.7: *Cutaway diagrams of eukaryotic cells showing the main organisational features and principal organelles. A: A generalised higher plant cell. B: A generalised animal cell. The DNA in eukaryotic cells is confined by inner membranes, the main part of the DNA is located in the nucleus, but smaller organelles such as chloroplast and mitochondria also hold their own DNA.*[69]

The general layout of a prokaryotic cell is shown in Figure 1.8. Prokaryotic cells, such as bacteria, lack the inner cells walls observed in eukaryotic cells and the prokaryotic DNA is therefore located in the cytosol. No resctictive membranes shield the prokaryotic DNA leaving it openly accessible to all components of the cytosol. This leads to significant differences in DNA related pathways and in the DNA structure. Eukaryotic DNA is linear and each cell contain several pieces of different DNA (chromosomes), while most prokaryotic cells contain a single circular chromosome. Telomere ends are present in eukaryotes to avoid shortening of the DNA during cell division (stem cells avoid this by expressing telomerase as described in Section 1.1), while the circular prokaryotic DNA has no need for telomeres. Telomere sequences are noncoding (not coding for any protein) and just 2% of eukaryotic DNA codes for proteins[72], while the number is 85–90% for prokaryotic DNA. Eukaryotic DNA is tightly packed in the chromatin, which is made up by the DNA and proteins related to the packaging. Prokaryotic DNA on the other hand is packed in a dense clump by super coiling without the aid of other proteins.[69]

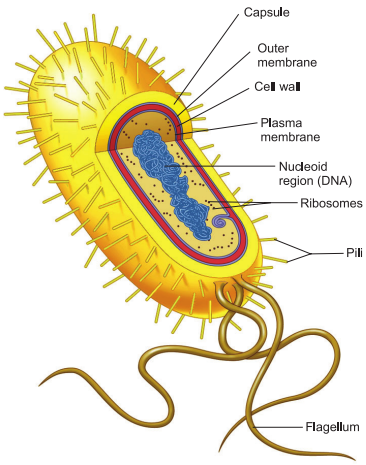

Figure 1.8: *Cutaway diagram of a generalised prokaryotic cell. The DNA in prokaryotic cells is located in the cytosol alongside all other macromolecules that have entered the cell membrane.* [69]

1.6 The Interaction Between DNA and Indolicidin

The interaction between indolicidin and DNA has classically been confirmed using gel retardation[73], but fluorescence quenching, surface plasmon resonance[9], crosslinking and mass spectrometric footprinting approaches has also been applied[11]. Indolicidin displays a high degree of structural plasticity with a globular and amphipathic conformation in aqueous solution, a wedge shape in membrane-mimicking environments, and presumably a third conformation related to DNA binding. The mechanism of interaction with DNA has been suggested as a two-state reaction model starting with electrostatic binding to the phosphate groups of the DNA duplex followed by insertion into the DNA groove[9]. The multiple positively charged amino acids suggest that indolicidin will bind strongly to the phosphate groups, and molecular dynamics simulations has suggested that indolicidin and indolicidin-4 will preferentially position itself in the major groove[74]. A sequence affinity has also been found showing a strong binding to ds[AT], ds[CG] and ds[AG], but only a weak binding to ds[GT].[9]

The binding of indolicidin to DNA hold the potential of inhibiting a large variety of DNA processing enzymes. A known example is the inhibition of topoisomerase I mediated relaxation of DNA[11]. The large size of the chromosome and the intense folding impose topological difficulties when essential enzymes require access to specific locations. The superhelical tension presents an obstacle that is overcome by topoisomerase I by breaking the DNA backbone, relaxing the strand and resealing the DNA[75]. The mechanism of topoisomerase I is shown in Figure 1.9.

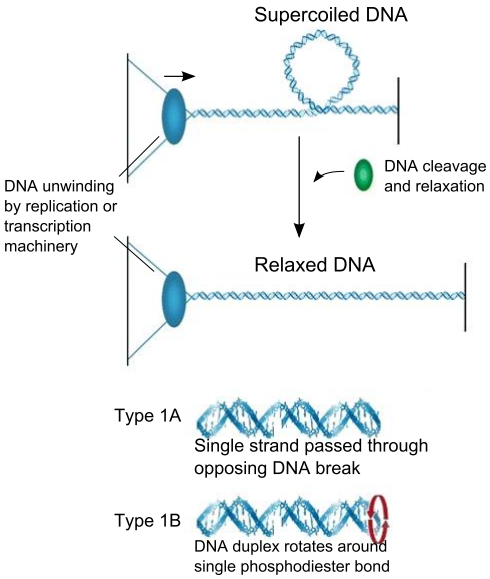

Figure 1.9: *The catalytic cycle of a type I topoisomerase: The enzyme binds to DNA, nucleophilic attack leads to cleavage of the DNA backbone, the DNA duplex is relaxed, the enzyme religates the DNA and dissociates. Adapted from Leppard et al.*[75]

Indolicidin has also been shown to bind covalently to abasic DNA sites[11]. Abasic DNA sites can be created spontaneously, under the action of radiations and alkylating agents, or enzymatically as an intermediate in the repair of modified or abnormal bases as the loss of a base leaving a deoxyribose residue[76].

1.6.1 Atomic Force Microscopy of the DNA-Indolicidin Interaction

AFM is one of few techniques that allows direct visualization of the DNA molecule, and it has the advantage of quick and simple sample preparation[77]. DNA can be imaged without the need for complex preparation methods that could alter the molecules biological function, making it possible to investigate the interaction between single DNA molecules and a wide range of proteins[78]. The preparations for imaging DNA with AFM are quick and simple, but they are of utmost importance for the experiment to mimic *in vivo* conditions, as the structure of DNA can be easily corrupted.

The conformation that DNA adopts when immobilised on a surface for AFM analysis depends on the environment and forces present during the binding process. A high concentration of salt[79] or dehydrating agents, such as ethanol[80], can cause a transition from B-form to A-form, and as such should be avoided. The binding of DNA to the surface must be strong enough to resist the motion of the moving tip during AFM scan, but not too strong as to change the conformation of the DNA. Mica is a reliable and convenient substrate for imaging of DNA as the crystal structure allows for perfect cleavage yielding a clean and smooth surface. The surface of mica is negatively charged and the binding of DNA can therefore be mediated by divalent ions, creating a reversible binding[81], or by a chemical modification of the surface

in order to mediate a covalent binding of the DNA such as with aminopropyltrimethoxysilane (APTMS).

Experimental Procedure 2

Relevant materials are listed in Appendix A.

2.1 Peptide Synthesis and Purification

Indolicidin (Cambridge Bioscience) with a purity of $\geq 95\%$ (HPLC peak area) was obtained and the two indolicidin analogs IL4 and IL4-RWT were synthesized by Fmoc (9-fluorenylmethyloxycarbonyl) solid phase peptide synthesis on rink amide resin. The peptides, abbreviation and amino acid sequence can be seen in table 2.1.

Peptide	Abbreviation	Sequence
Indolicidin	IL	ILPWKWPWWPWRR
Indolicidin-4	IL4	ILPWKLPLLPLRR
Indolicidin-4 + fluorophore	IL4-RWT	ILPWKLPLLPLRR(Acx)[1](Rwt)[2]

Table 2.1: *Peptides obtained for use in the project. Common name or description in column 1, abbreviation in column 2 and amino acid sequence in column 3.* [1]*Amino hexanoic acid.* [2]*Rhodamine water tracer.*

2.1.1 Solid Phase Peptide Synthesis

The peptide IL4 was synthesised with a theoretical yield of 0.615 mmol and 20%, corresponding to 0.123 mmol, of the product was afterwards used to synthesise IL4-RWT. Synthesis was done following the Fmoc/tBu approach as described by Chan and White[82]. An aminomethyl resin with a loading capacity of 1.23 mmol/g was utilised and 3 equivalences of Fmoc-amino acids (AnaSpec) with appropriate side chain protection were used for each coupling. The resin was washed 3 times with DCM, DMF and MeOH, and swelled in DCM for 20 minutes before each coupling step. Deprotection was carried out using 2 steps of 10 minutes mixing with 10 mL/mmol 20% piperidine/DMF follow by 3 times DCM/DMF wash and a ninhydrin test[83] for primary amines and a chloranil test[84] for proline. Amino acids with 1.0 equivalence of Oxyma were dissolved in 10 mL/mmol DMF and activated for 10 minutes using 1.0 equivalence of DIC. Couplings were then performed with 360° mixing for 3 hours at room temperature followed by a ninhydrin or chloranil test.

20% of the product was removed after coupling the last amino acid of IL4, and the spacer 6-(Fmoc-amino)hexanoic acid as well as the fluorophore rhodamine water tracer were coupled following the above procedure.

Deprotection of both peptides and cleavage from the resin was performed by treatment with 10 mL/mmol of a TFA/TIS/DCM mixture (90:5:5) for 120 minutes with 360 ° mixing. The peptide was then precipitated by three steps of adding -20 °C diethyl ether, mixing, 10 min centrifugation at 10,000 G and decantation. The precipitates were finally vacuum dried and stored at -20 °C. Cleavage was done on resin-peptide after the coupling of the first 13 amino acids and a deprotection, and after the coupling of spacer and fluorophore. A preliminary small-scale cleavage of peptide-resin was initially carried out using 1 mg of the product, where after the full amount was cleaved.

2.1.2 RP-HPLC Analysis and Purification of Synthesised Peptides

Products from synthesis of IL4 and IL4-RWT were analysed and purified using reverse-phase high performance liquid chromatography (RP-HPLC). The mobile phase was composed of a H_2O with 0.1% (v/v) TFA and acetonitrile gradient.

Analysis was done on a Dionex Accalaim C18 reversephase column (4.6 mm x 150 mm, 3 µm, 300 Å) by loading 100 µL 0.1% (w/v) TFA in H_2O with a small amount of synthesis product dissolved. A flow rate of 1 mL/min and a linear gradient from 5 to 80% acetonitrile was applied for both peptides. An absorption spectrum from 214 to 600 nm in 2 nm steps was recorded.

Purification was done on a Dionex Gemini-NX C18 reverse-phase column (10.00 mm x 250 mm, 5 µm, 110 Å) by loading 2 mL 0.1% (v/v) TFA in H_2O with a larger amount of synthesis product dissolved. The amount of dissolved product was adjusted to a level ensuring proper peak seperation. Absorbance at 280 nm was used for fraction collection of IL4 and 554 nm for fraction collection of IL4-RWT. The collected fractions were freeze-dried and stored at -20 °C.

2.1.3 Mass Spectrometry

Mass spectrometry was performed using a Bruker Reflex III reflectron MALDI-TOF instrument (Bruker Daltonik, Germany). A small fraction of the collected product from RP-HPLC was dissolved in a matrix-solution composed of 3g/L 2,5-dihydroxy benzoic acid (Sigma) in acetonitrile and 0.1% TFA in water (1:1). 1 µL solution was deposited on a sample support and left to dry before loading into the mass spectrometer. External calibration was performed prior to analysis using a pepmix calibrant mixture (Bruker).

Data was analysed in Mmass[85,86] and plotted in Matlab.

2.2 Maintenance of hESC

Established human embryonic stem cell lines were sustained and augmented in a feeder free medium. The cells were maintained in 6 well culture plates (Corning, Lowell, MA) coated with Matrigel^{TM} (BD Biosciences). RH1 cells were grown in mTESR® 1 (StemCell Technologies) medium added 1% penicillin, 1% streptomycin and 1% fungizone. T8 cells were grown on similar medium however with the addition of 0.1% G418 (Life Technologies). Cells were maintained at a temperature of 37 °C and CO_2 concentration at 5%.

The cells were fed every day by aspiration of the old medium and careful addition of 2 mL 37 °C new medium. The cells were routinely passaged as well as treated to maintain an undifferentiated state. All work was performed using aseptic conditions in a laminar flow hood.

Passaging of cells

The cells were monitored under microscope daily and passaged when a confluency of 90-100% was reached. Passaging was done approximately every 5 days. 1 mL Matrigel stock solution (see Appendix A) was added to each well of the 6-well culture plate and left to settle at room temperature for at least one hour. Excess Matrigel was aspirated and 1 mL media added shortly before cells were plated. The well containing cells was aspirated, carefully added 2 mL 37 °C PBS, aspirated and added 1 mL of room temperature collagenase solution (see Appendix A). The plate was then incubated at 37 °C for 5 minutes or until the colony edges started to loosen. Collagenese was aspirated and the well carefully washed with 2 mL 37 °C PBS before 2 mL medium was added. The cells were then carefully scraped off the well using a small cell scraper (Corning, Lowell, MA). The medium containing cells was then added to the newly prepared wells; one well of RH1 was added to two new wells, while each well of T8 was added to three new wells. An additional 1 ml medium was used to wash remaining cells of the old well and transfer them to the new wells. All wells were added medium to a final volumen of 2 ml before immediately being moved to the incubator.

Selection of undifferentiated cells

Cells with ES like morphology were isolated to promote the undifferentiated state of the cells, when other morphologies became apparent. Areas of non ES like morphology were identified and removed using a scraper and a localized continuous flow of 37 °C PBS. The remaining cells were afterwards passaged.

Haircut

The haircut method was used when colonies of different morphologies were not separatable. The well was aspirated, added 1 mL room temperature collagenase and incubated for approximately 3 minutes at 37 °C. The collagenase was then aspirated and 37 °C PBS was carefully passed over the cells until cells

of non ES morphology were washed off. The well was then aspirated, added 2 mL media and incubated for at least 24 hours before further passaging.

2.3 Preparation of Single cell Suspension

Single cell suspensions were used in experiments where cell lumps were unfavourable and where cell count was required. Each well of the 6-well culture plate was aspirated, carefully added 2 mL 37 °C PBS, aspirated and added 1 mL 37 °C 0.025% Trypsin/EDTA solution (see Appendix A). The plate was then incubated at 37 °C for 5 minutes or until the cells were dislodged. 2 mL media was added to neutralize the enzyme, and the cells were harvested and dispersed to a single cell suspension using a serological pipette. The cells were then transferred to a falcon tube and centrifuged at 200g for 5 minutes at room temperature. The media was aspirated and the cell pellet resuspended in 2 mL 37 °C media previously added 0.1% ROCK inhibitor (Millipore). 20 µL of the cell suspension was mixed with 60 µL Trypan blue (Invitrogen) and the cells were counted a minimum of three times using a hemocytometer. The cell suspension was then diluted to the desired concentration in media with 0.1% rock inhibitor and added to Matrigel coated wells.

2.4 Preparation of peptide containing medium

Media containing IL, IL4 or IL4-RWT for experiments were prepared in advance and stored for up to 7 days at 5 °C. Peptides were dissolved in PBS and the concentration measured using A_{280} and A_{590} on a NanoDrop 1000 Spectrophotometer (Thermo Scientific, Waltham, Massachusetts). The solvated peptides were added to the desired medium in less than a 1:100 ratio and the solution was filter sterilised.

2.5 Cell Viability Assay

Cell viability assay were performed based on an optimised protocol of the CellTiter-Blue™ Cell Viability Assay[87]. 96 well cell culture microplates (Greiner Bio-one) were prepared by addition of 30 µL Matrigel to each well followed by incubation at room temperature for atleast one hour. The Matrigel was then removed and each well washed with 200 µL PBS. RH1 and T8 single cell suspensions were concurrently prepared and 10,000 cells in 200 µL media with 0.1% ROCK inhibitor seeded in each well.

Media containing different concentrations of peptide was prepared as described above. The starting me-

dia was removed from all wells after 24 hours and 200 µl 37 °C peptide containing media was added to each well. This was repeated at 72, 120 and 168 hours.

Measurements were performed after 192 hours or when any well in a plate reached confluency. The media was removed, all wells washed with 200 µL PBS and added 100 µL PBS and 20 µL Cell-Titer Blue (Promega, Madison, WI) previously mixed and heated to 37 °C. The plate was incubated for 2 hours at 37 °C and fluorescence recorded with excitation/emission at 560/590 nm using an automated plate reader with excitation applied from the bottom and emission acquired likewise from the bottom.

2.6 Measurement of IL4-RWT cellular uptake

RH1 embryonic stem cells were used for screening of peptide uptake. 100,000 cells were passaged into each well of a 12 well plate as described in section 2.3. The media was replaced with new 37°C media 24 hours after passaging, and medium containing 5 µg/mL IL4-RWT was prepared and kept at 37°C. Wells were then incubated with IL4-RWT media at different time points by aspiration of the existing media, wash with 37°C PBS and addition of 1 mL 37°C of the IL4-RWT media. The time points corresponded to final incubation times of 24, 12, 3, 2, 1, 0.5 and 0.25 hours. The cells were monitored using phase contrast microscopy and fluorescence confocal laser scanning microscopy.

The cells were harvested by aspiration of the media, two times wash with PBS and addition of 0.5 mL 37°C 0.025% Trypsin/EDTA solution followed by 5 minutes incubation at 37°C. 1 mL ice cold FACS PBS solution was then added and the cells were collected and dispersed to a single cell suspension using a serological pipette. The cells were transferred to a falcon tube and collected by 5 minutes centrifugation at 200g before resuspension in ice cold FACS PBS (PBS + 1% FBS). Centrifugation and resuspension was performed twice with final resuspension in 500 µL. Cells were then kept on ice and used shortly after for flow cytometric analysis on a FACSCalibur (BD Biosciences, Bedford, MA) flow cytometer.

Flow cytometry data was analysed using FCS Express 4 (De Novo Software).

2.7 RH1 in mTeSR Differentiation Assay

The effect of indolicidin-4 on RH1 embryonic stem cells growing on mTeSR medium was examined. 100,000 RH1 cells were passaged into each well of a 12 well plate, as described in section 2.3, and incubated for 24 hours. mTeSR with 50 µg/mL IL-4 was prepared as described in section 2.4 and 3 wells were subjected to treatment by growth on mTeSR or mTeSR IL-4 medium for 5 days with daily replacement of the media. Morphology was monitored daily using a phase contrast microscope and total

RNA was isolated after the 5 days treatment as described in Section 2.10.

2.8 T8 in mTeSR Differentiation Assay

The effect of indolicidin and indolicidin-4 on T8 embryonic stem cells growing on mTeSR medium was examined. The T8 cell line is a tranfected human embryonic stem clonal cell line expressing EGFP under control of the Oct-4 promoter[23].

Six different media were prepared based on the mTeSR®Basal Medium (StemCell Technologies,Vancouver, Canada) and the mTESR®1 5X Supplement without Select Factors (StemCell Technologies). A positive control was prepared by addition of the following select factors: 0.6 µg/mL Recombinant Human TGF-β1 (R&D Systems), 0.1 µg/mL bFGF, 42 µg/mL Lithium Chloride, 129.7 ng/mL pipecolic acid and 103.1 ng/mL γ-aminobutyric acid (GABA). The positive control mimics the fully supplemented mTeSR. A negative control was prepared without addition of any select factors. An intermediary medium was prepared as the positive control but without addition of TGF-β. Three constrained media were prepared be exclusion of TGF-β and bFGF, and from these media one was added 50 µg/mL IL4 and one 20 µg/mL IL. The select factors and peptide additions to each media is listed in Table 2.2

Description	bFGF	TGFβ	LiCl	PA	GABA	IL	IL4
Positive control	■	■	■	■	■		
Negative control							
-bFGF/TGFβ			■	■	■		
-bFGF		■	■	■	■		
+IL11			■	■	■	■	
+IL4			■	■	■		■

Table 2.2: *Media conditions used for the T8 in mTeSR differentiation assay. mTESR®1 Basal Medium and mTESR®1 5X Supplement without Select Factor were used as basis and select factors or peptides were added: Recombinant Human TGF-β1 (TGF-β), basic fibroblast growth factor (bFGF), Lithium Chloride (LiCl), pipecolic acid (PA), γ-aminobutyric acid (GABA), indolicidin (IL) and indolicidin-4 (IL4). Added constituents are marked with* ■ .

1,000 T8 cells were passaged into each well of a 96 well plate and 30,000 cells into each well of a 6 well plate, as described in section 2.3, and incubated for 24 hours. 24 wells of the 96 well plate and 1 well of the 6 well plate were subjected to treatment by growth on each of the six different media for 7 days with daily replacement of the media. 4 wells of the 96 well plate of each condition were removed and analysed every 24 hours starting just prior to the transition from mTeSR to the six different media. Analysis was done by addition of 20 µL 10x Hoechst stain in PBS for a final concentration of 2 µg/mL and incubation at 37 °C for 20 minutes before aspiration, addition of 200 µL PBS, aspiration and a final addition of 200 µmL PBS. The fluorescence signal of each well was measured using an automated plate reader with 485/510 and 350/470 excitation/emission filters, excitation and emission applied from the bottom. Morphology was monitored daily using a phase contrast microscope.

The cells of each of the six media conditions in the 6 well plate were passaged when the positive control reached 90% confluency. 30,000 cells of each condition were trypsin passaged into a new well of a 6 well plate and 1,000 cells were passaged into each well of a 96 well plate. Remaining cells pellets were collected by centrifugation at 250g, aspiration of the media and a snapfreeze of the pellet to -80 °C. Total RNA was isolated for real-time reverse-transcription PCR as described in section 2.10. 4 wells of the 96 well plate of each condition were removed and analysed every 24 hours by a capture of green and blue fluorescence images of 3 areas of each well and cells were counted as described in Appendix C.

Passaging of the cell in the 6 well plate to new 6 well plates was performed a further two times for a total of four passages. Remaining cells pellets were collected for RNA isolation.

2.9 RH1 in E8 Differentiation Assay

The effect of indolicidin and indolicidin-4 on RH1 embryonic stem cells growing on the fully defined E8 medium was examined. RH1 cells had been previously transitioned from mTeSR to E8.

E8 medium was prepared as described by Thomson et al.[27] with the extra addition of 1% penicillin, 1% streptomycin and 1% fungizone. E6 medium was prepared as E8 but without the addition of insulin and TGFβ. E8 medium containing 50 μg/mL IL-4 or 20 μg/mL IL was prepared as described in section 2.4. 100,000 RH1 cells were passaged into each well of a 12 well plate, as described in section 2.3, and incubated for 24 hours. 4 wells were used for each of the five media conditions: E8, E8 + IL4, E8 + IL and E6, and each well was treated for 5 days with daily replacement of the media. Morphology was monitored daily using a phase contrast microscope and total RNA was isolated after the 5 days treatment as described in section 2.10.

2.10 Real-Time Reverse-Transcription PCR

Real-time reverse-transcription PCR was used for quantification of mRNA transcription levels.

Total RNA was extracted from cells using the TRIzol®Reagent (Invitrogen) according to the manufacturer's instructions. RNA concentration was determined using a NanoDrop 1000 Spectrophotometer and 0.5 μg RNA was reverse transcribed using oligo$(dT)_{20}$ (Invitrogen) primers and the Superscript®III RT First-Strand kit (Invitrogen). A negative control, without addition of the enzyme, was always included, and cDNA purity was confirmed by 2% agarose gel electrophoresis after performing PCR using GAPDH primers and the Biotaq^{TM} Red DNA Polymerase kit (Bioline). RQ1 RNase-Free DNase (Promega) was applied to extracted RNA when required.

cDNA was quantified using the Dynamo Flash SYBR®Green qPCR kit F-415 (New England Biolabs) and a PTC-200 cycler with a Chromo-4 detection system (MJ Research). Each reaction was performed using 0.5 ng cDNA in a final volumen of 20 µl with 200nM forward and reverse primer. The amplification profile consisted of 7 min initial denaturation at 95 °C, followed by 40 cycles of 15 s 95 °C denaturation and 30 s 59 °C combined annealing and extension. Melting curves were finally aquired by a 0.5 °/min increase in temperature from 65 to 95 °C.

Primers for GAPDH, Oct-4 and Nanog had previously been designed for a melting temperature of 64 °C.

2.11 Maintenance of Human Dermal Fibroblast

Human dermal fibroblast of neonatal foreskin origin were sustained and augmented for isolation of DNA. The cells were grown in T75 flasks (BD Biosciences, Bedford, MA) in 10 mL Medium 106 added Low Serum Growth Supplement (Invitrogen). Passaging of the cells was performed by aspiration of the media, wash with 37 °C PBS and addition of 4 mL 37 °C 0.025% Trypsin/EDTA solution followed by 2 minutes incubation at 37 °C. 6 mL media was added to neutralize the enzyme, the cells were harvested and then transferred to a falcon tube for 5 minutes centrifuged at 200g. The media was aspirated and the cell pellet resuspended in 8 mL 37 °C media. 2 mL cell suspension along with 8 mL 37 °C media was added to each of four new T75 flasks and the flasks placed in the incubator. Passaging was performed every 3-5 days. The cells were fed every other day by aspiration of the old medium and addition of 10 mL 37 °C new medium.

2.12 Fragmentation of DNA

DNA was isolated from RH1 and HDF cells using the DNeasy® Blood & Tissue kit (Qaigen). RNase A (Invitrogen) was applied as suggested in the protocol. The DNA was subsequently fragmented and purified. Concentration was measured as $A_{280} \times 50$ µg/mL.

2.12.1 Fragmentation of DNA by Sonication

Ultrasonification was done using a Branson 2510 ultrasonic cleaner (Emerson Industrial Automation, St. Louis, Missouri) that generates a frequency of 45 kHz. 10 µg DNA in 200 µL DNAse free H_2O was loaded in 1.5 mL reaction tubes (Greiner bio-one) for a final concentration of 50 µg/mL (∼33 µM). The test tubes were submersed so the inner solution was at level with the water of the tank. Sonication was applied in 1 minute intervals interspersed by mixing and collection by brief centrifugation. The

temperature was maintaned at 25 °C throughout the procedure.

2.12.2 Restriction Enzyme Digestion of DNA

A ten-fold overdigestion with the restriction endonucleases EcoRI (Fermentas) and XhoI (Fermentas) were used to digest DNA. 10 µg DNA was digested using 200 U EcoRi, 200 U XhoI and the Tango™ Buffer (Fermentas) in a total volume of 200 µL for 3 hours at 37 °C. The digested mixture was subsequently EtOH precipitated.

2.12.3 EtOH Precipitation

EtOH precipitation of DNA was performed by adding 1/10 volume of 3 M NaAc, pH 5.2, and 2 volumes of 96% ethanol to the DNA solution, incubating the mixture at -20 °C and centrifuging for 30 minutes at 20,000 g and 4 °C. The supernatant was carefully decanted, 1 volume 70% ethanol was added and the mixture centrifuged for 10 minutes at 20,000 g and 4 °C. The pellet was air dried before dissolving in DNase free H_2O.

2.12.4 Agarose Gel Electrophoresis

Electrophoresis was used to analyse and purify DNA fragments. Gels were prepared by dissolving 1% or 2% agarose (Sigma) in 1x TAE buffer (GibcoBRL), heating to 65 degrees, adding 1 µL EtBr and cooling in a cast. The gel was placed in a 1x TAE buffer and samples were prepared by mixing DNA with 6x loading dye (Fermentas) and DNase free H_2O before depositing in the gel. 50 bp or 1 kbp DNA Generuler™ ladders (Fermentas) were used as reference. 50 V (5 V / cm) was applied for 90 minutes and the gel was imaged using UV exposure.

2.13 DNA Immobilisation on APTMS Coated Mica Surface

Chemical vapour deposition of 3-aminopropyltrimethoxysilane (APTMS) (Sigma Aldrich) was used to functionalise a mica surface for DNA binding. High quality muscovite mica (Electron Microscopy Sciences) was cleaved using an adhesive tape and placed in a desiccator next to a solution of APTMS in toluene (1:3). The desiccator was evacuated to approximately 50 mbar, briefly flushed with argon and evacuated before leaving for 20 minutes. The APTMS treated surfaces were used immediately after treatment.

DNA from the human cells RH1 and HDF was prepared as previously described and the recombinant plasmid cloning vector pUC19 (2686 bp) (Fermentas) was obtained for comparison. A 20 mM ammo-

nium acetate buffer, adjusted to pH 5.2 by hydrogen chloride, was prepared by filtration through a 0.2 μm filter (Sartorius Stedim Biotech) and brief centrifugation. DNA was diluted to approximately 1.25 μg/mL (A_{280}=0.025 equaling 1.89 μM) in the ammonium acetate buffer and 40 μL was deposited on the freshly prepared mica surface. The sample was incubated for 10 minutes at room temperature, the surface gently washed with 1 mL DNase-free H_2O and dried under a stream of N_2.

A variation of the procedure was performed by preparing 10 μL 50 μg/mL IL4 or IL4-RWT, depositing it on the DNA drop after 5 minutes of incubation and gently mixing using a 100 μL pipette. The procedure was then completed by the last 5 minutes of incubation, wash and drying.

2.14 High-resolution Atomic Force Microscopy

High-resolution topographies were produced using a Digital Instrument Nanoscope IIIa Multimode (Digital Instruments/Veeco, Santa Barbara CA, USA) equipped with an J scanner having a maximum scan area of 120 μm x 120 μm. The AFM was operated in tapping mode. A scan rate of 0.5 Hz and a maximum scan velocity of 2 μm/s were used. Cantilevers used were OMCL - AC200TS (Olympus) with a nominal spring constant of 9 N/m and a working frequency at approximately 150 kHz. All topographies were captured as 512 x 512 pixel images.

Topographies were plan subtracted and flattened using the WSxM 5.0 Develop 1.0 software[88].

Results 3

3.1 Peptide synthesis and purification

The peptides IL4 and IL4-RWT were synthesised using an Fmoc solid phase approach. The products were quantitatively analysed and purified using reversed-phase high-performance liquid chromatography and MALDI-TOF mass spectrometry was performed on isolated fractions for qualitative analysis.

3.1.1 Synthesis procedure

Synthesis of IL4 was performed with a theoretical yield of 0.615 mmol. The effectiveness of each deprotection and coupling step was confirmed with a ninhydrin test for primary amines and a chloranil test for proline. Deprotected N-terminus showed as a dark blue color, while a complete coupling yielded a colorless or brownish result. The coupling step was repeated when the ninhydrin or chloranil test was positive, and coupling times were adjusted corresponding to results obtained in the first couplings. The following synthesis of IL4-RWT was performed with a theoretical yield of 0.123 mmol and the effectivity of each deprotection and coupling step was confirmed with a ninhydrin test.

A small-scale cleavage of peptide-resin was performed on both IL4 and IL4-RWT synthesis products to ensure proper couplings. Mass spectrometry of IL4 and IL4-RWT yielded only one significant peak each: 1614 and 2198. Further analysis was performed after cleaving the remaining peptide-resin.

3.1.2 RP-HPLC Analysis and Purification of Synthesised Peptides

The synthesis products were analysed using RP-HPLC. The analytical chromatogram obtained for the product of the IL4 synthesis is shown in figure 3.1. The acetonitrile concentration was increased linearly from 0 to 80% and the concentration corresponding to the measured absorption is plotted in the figure. One main peak was observed at a retention time of 30.15 to 31.48 minutes (38.15 to 38.48 % ACN) at both 214 and 280 nm, while minor peaks were present at higher concentrations. The area of the main peak at 214 nm contained the main part of the measured absorption. Collection of the main peak in suqsequent runs were based on the 280 nm signal.

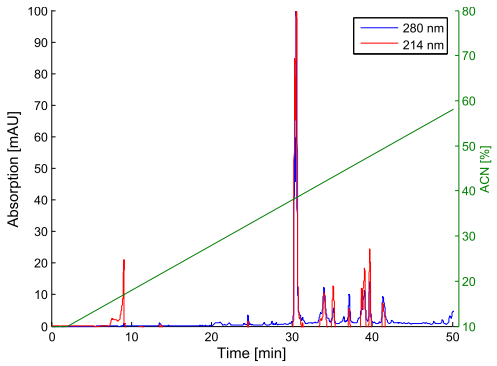

Figure 3.1: *Analytical chromatography of IL4. A main peak is observed at a retention time of 30.15 to 31.48 minutes (38.15 to 38.48 % ACN).*

The analytical chromatogram obtained for IL4-RWT is shown in figure 3.2. The absorption at wavelengths 214 nm, 280 nm and 550 nm are plotted, and all wavelengths showed a main absorption at a retention time of 40 to 50 minutes (36.2 to 43.1 % ACN). Three peaks were observed at 550 nm, and the two major peaks were used for suqsequent fraction collection. The two peaks are believed to correspond with the two isomers of rhodamine water tracer[89].

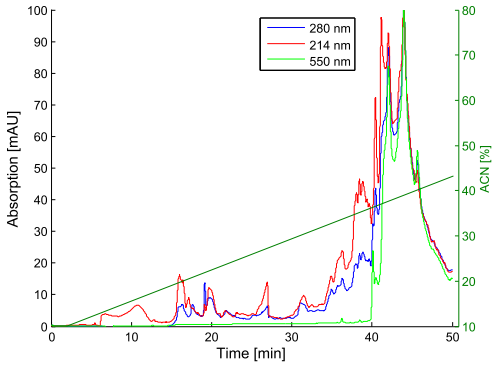

Figure 3.2: *Analytical chromatography of IL4-RWT. Main peaks are observed at retention time 40 to 50 minutes (36.2 to 43.1 % ACN)*

3.1.3 Mass Spectrometry

Figure 3.3 shows the mass spectrum of the eluent obtained from RP-HPLC collection of the IL4 synthesis product. The eluent corresponded to the main peak observed in Figure 3.1. The only significant peaks in Figure 3.3 (A) were located around a m/z of 1614 and (B) shows an isotope distribution from 1614 to 1617. Mass spectrometry was performed with a positive ionisation, and the monoisotopic mass with H^+ ionisation was calculated (using GPMAW[90]) to 1614.073 g/mol. The monoisotopic mass correlates with the first peak in the isotope distribution.

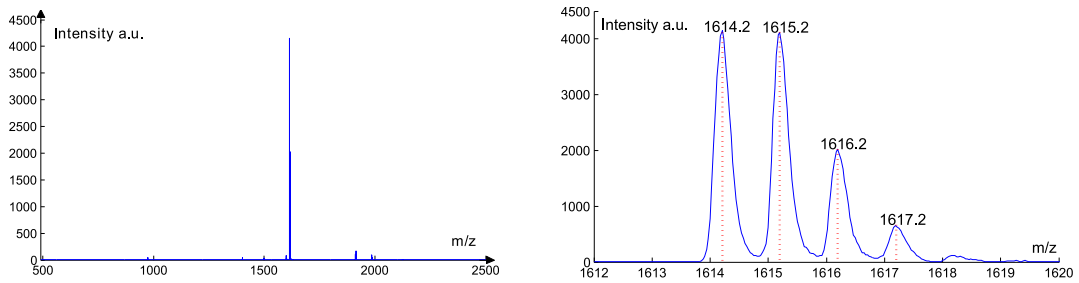

Figure 3.3: *MALDI-TOF spectrum of the main RP-HPLC fraction from IL4 synthesis. (A) shows the spectrum from m/z 500 to 2500 while (B) shows that the major peak consist of an isotope distribution with the first peak corresponding to the monoisotopic mass of IL4 with H^+ ionisation (1614.073 g/mol).*

The monoisotopic mass of IL4-RWT was calculated as 2197.35 g/mol. The mass spectrum of the IL4-RWT synthesis product (not shown) yielded a main peak corresponding to an isotope distribution of IL4-RWT with H^+ ionisation.

3.2 Cell Viability Assay

Cytotoxicity of the peptides indolicidin, indolicidin-4 and indolicidin-4-RWT was tested on the ES cell lines RH1 and T8. The cell viability assay was based on a mTESR and Matrigel system with growth for 7 days or until confluency was reached. mTeSR was used as positive control, while PBS and 50% DMSO/PBS were used as negative controls. Background correction was performed by substracting the fluorescence of wells with no added cells, but otherwise the same conditions.

Plots of the obtained cell viability values are inluded in Appendix B. The cytotoxic concentration was determined as the concentration of peptide that yeilded no apparent resorufin fluorescence at the end of the assay and caused a complete loss of cell growth, as determind visually by phase contrast microscope. IL was cytotoxic at $\geq$ 100 µg/mL, IL4 at $\geq$ 333 µg/mL and IL4-RWT at $\geq$ 100 µg/mL. Similar values were obtained for both cell lines.

Peptide	**Cytotoxic concentration**
Indolicidin	100 µg/mL
IL-4	333 µg/mL
IL4-RWT	100 µg/mL

Table 3.1: *Cytotoxicity of IL, IL4 and IL4-RWT. The cytotoxic concentration was determined as the concentration at which a 100% reduction in fluorescence is observed with the CellTiter-Blue^{TM} Cell Viability Assay.*

3.3 Measurement of IL4-RWT cellular uptake

The uptake of the peptide IL4-RWT into living RH1 embryonic stem cells was tested using flow cytometry and high resolution microscopy. Flow cytometry was used to determine the kinetics of cell uptake of the peptide while fluorescence confocal laser scanning microscopy was used to estimate the intracellular location of the peptide. Phase contrast microscopy with wide-field fluorescence overlay showed a small fluorescent signal from the Matrigel surface and the fluorescence intensity did not increase visibly from 0.25 hours to 24 hours incubation time. Figure 3.4 A shows a phase contrast microscopy image of RH1 cells after 1 hour of incubation with 5 µg/mL IL4-RWT in mTeSR followed by wash with PBS. The same area was imaged with fluorescence illumination (B) and the signal has been overlayed (C) to show the correlation between cells and fluorescence. Two different morphologies are observed in the phase contrast image, the upper consist of compactly packed cells in a well-defined colony resembling ES cells, while the lower consists of dispersed flat cells resembling differentiated cells. The fluorescence intensity matches the cell density with the highest density of fluorescence located at in the dense colony, while the dispersed non-ES like cells only show a low level of fluorescence.

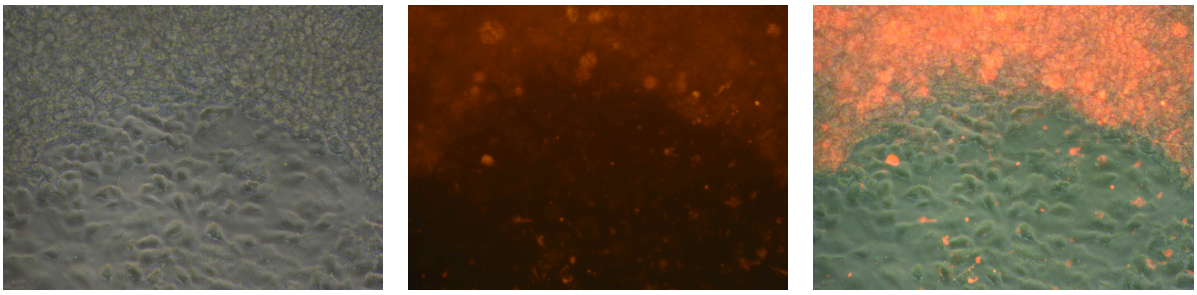

A B C

Figure 3.4: *RH1 embryonic stem cells incubated with 5 µg/mL IL4-RWT in mTeSR. A) shows a phase contrast microscopy image of an ES-like colony and adjacent non-ES-like cells. B) shows a red fluorescence image captured of the same area and C) shows the overlay.*

Confocal laser scanning microscopy was used to investigate if the peptide was located only on the cell surface or if there was a specific intracellular preference. Figure 3.5 shows images from a z-stack of RH1 cells after 1 hour incubation with 5 µg/mL IL4-RWT in mTeSR followed by wash with PBS. The reflection and fluorescence signal are merged to show the intracellular location of the peptide. The fluorescence was generally poorly distributed between cells, and areas with intense fluorescence was observed on the Matrigel surface. A cell with a uniform intracellular distribution of fluorescence can be seen in the center of the images and no intracellular preference was generally observed.

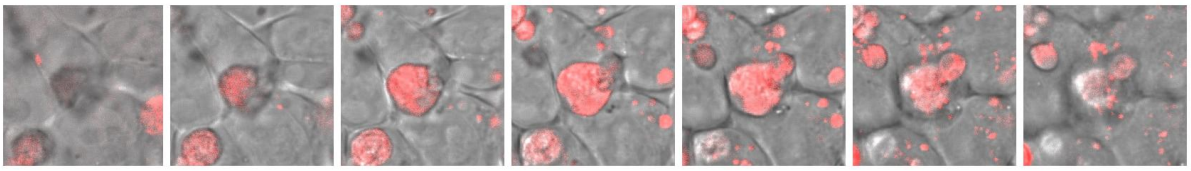

Figure 3.5: *Intracellular location of the peptide IL4-RWT as demonstrated by confocal laser scanning microscopy. Seven z-positions of the merged reflection and red fluorescence signal show the distribution of peptide through the cell.*

Flow cytometry was used to quantitatively evaluate the cell uptake of IL4-RWT by measuring the fluorescence intensity from a large number of cells. Forward scatter (FSC) correlates with the size of cells while side scatter (SSC) correlates with internal complexity of cells, and a gating profile - previosuly matched to living embryonic stem cells - was applied using said detectors. Figure 3.6 (A) shows the FSC/SSC plot of the reference sample, added no IL4-RWT, and the gating profile "ES cells". The distribution of cell count obtained at different fluorescence intensities using a red fluorescence filter, and applied the gating profile, is shown in (B).

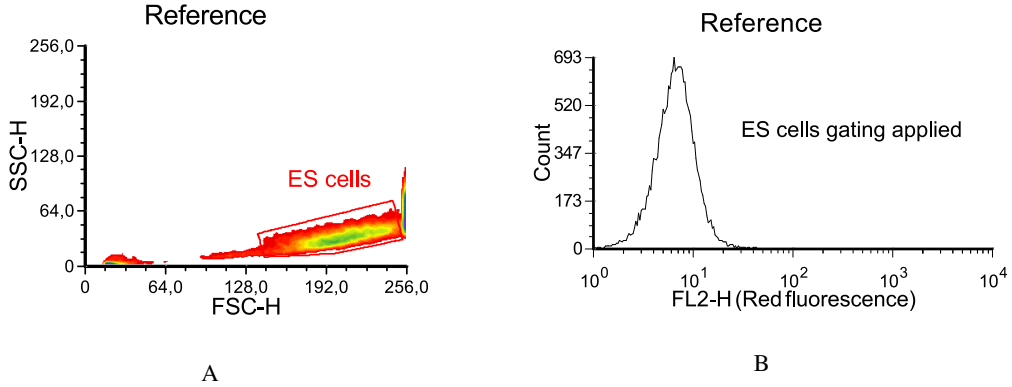

Figure 3.6: *Flow cytometry analysis of RH1 ES cells. The "ES cells" gating is shown in A and the red fluorescence intensities of the cells within the gating is given in B.*

The same gating was applied to all samples and Figure 3.7 shows the distribution of cell count obtained at different fluorescence intensities for the eight samples of increasing incubation time.

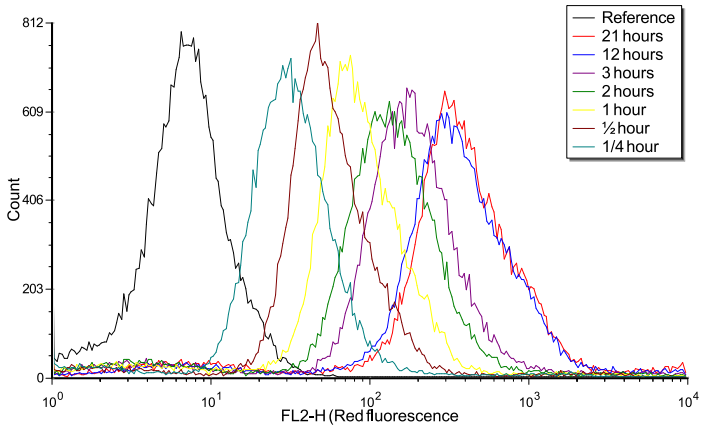

Figure 3.7: *Flow cytometry analysis of RH1 ES cells. The distribution of cell count obtained at different fluorescence intensity is plotted for the eight samples of increasing incubation time.*

The cell count before and after application of the gating and the median of fluorescence intensity of each sample is listed in Table 3.2.

Incubation time (h)	Total events	Gated events	Median
0	28,110	19,050	6.45
0.25	26,478	19,096	30.51
0.5	26,413	18,516	50.48
1	27,068	19,028	80.58
2	27,140	19,034	128.64
3	27,097	19,186	171.54
12	27,305	15,932	339.82
24	27,474	17,064	352.27

Table 3.2: *Summary of flow cytometry data for RH1 ES cells incubated with IL4-RWT. The amount of observed cells before and after application of the "ES Cell" gating and the median of fluorescence intensity is given for all samles of different incubation time.*

The relative transduction efficiency was calculated from the median of fluorescence intensity. The reference with an incubation time of 0 hours was used as background and the sample of 24 hours incubation was used as 100% transduction. The relative transduction as a function of incubation time is plotted in Figure 3.8.

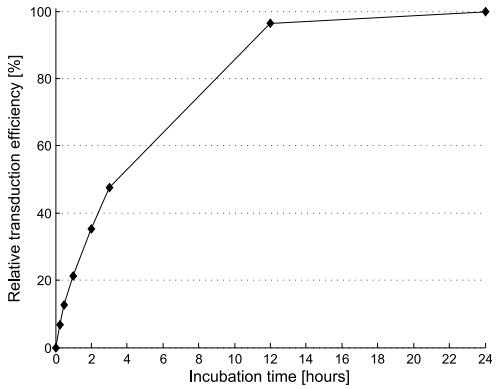

Figure 3.8: *Uptake kinetics of the peptide IL4-RWT. RH1 cells were incubated with 5 µg/mL IL4-RWT in mTeSR at 37 °C for 0.25, 0.5, 1, 2, 3, 12 and 24 hours. The cells were harvested and analysed by flow cytometry at the indicated time points. A saturation of uptake is achieved around 12 hours.*

100% transduction, as seen at 24 hours incubation, equals a 50 fold increase of fluorescence compared to the untreated sample. Saturation is achieved around 12 hours incubation.

3.4 RH1 in mTeSR differentiation assay

The effect of 50µg/mL IL4 in mTeSR was tested on RH1 embryonic stem cells by 5 days growth and analysed by comparison with cells growing on mTeSR. A qualitatively analysis of the cell morphology was performed using a phase contrast microscope, and consistensy between the biological replicates was observed for both media conditions. Figure 3.9 shows the general morphology after 5 days growth for both media conditions. The confluency is 95% to 100% and both conditions show almost only ES-like morphology. No apparent difference is visible for the two conditions.

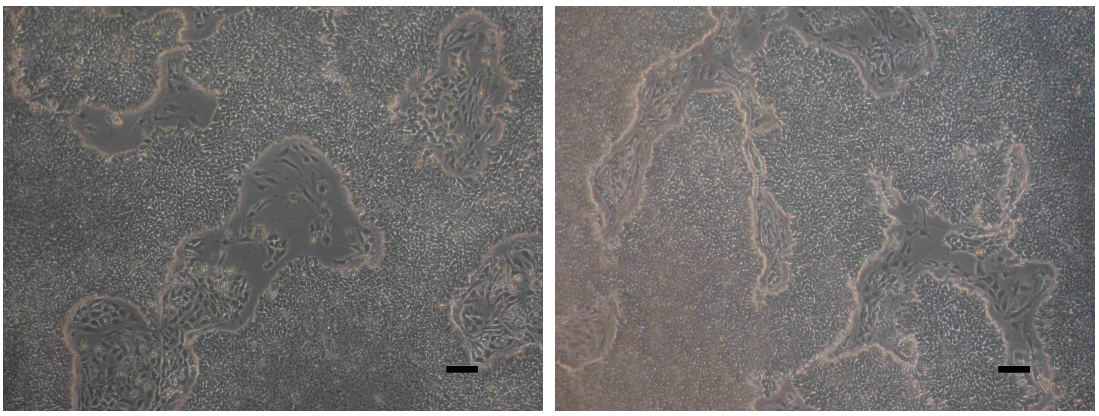

A B

Figure 3.9: *RH1 morphology after 5 days growth in (A) mTeSR and (B) mTeSR + 50µg/mL IL4. Both conditions have reached 95%-100% confluency and show almost only ES-like morphology, while few non-ES like cells are present between colonies. Scale bar, 100 µm.*

Oct-4 and Nanog are pluripotency transcription factors and the expression of these genes are often used

to characterise embryonic stem cells. The expression of the two genes was measured as the amount of mRNA in the cell by isolating the total RNA, reverse transcribing to complementary DNA and quantifying by real-time PCR. The housekeeping gene GAPDH was used as endogenous control to calculate the change in relative expression of Oct-4 and Nanog. A detailed description of the reaction and data processing are included in Appendix D.

Real-time reverse-transcription PCR was performed on the three biological replicates of each condition, and three technical replicates were used in the PCR procedure. The relative change in Oct-4 and Nanog expression compared to the RH1 cells growing on mTeSR is shown in Figure 3.10. A significant increase in Oct-4 expression can be observed (22% increase with $\sigma = 13\%$) while the expression of Nanog seems unaffected by the addition of indolicidin to the growth media.

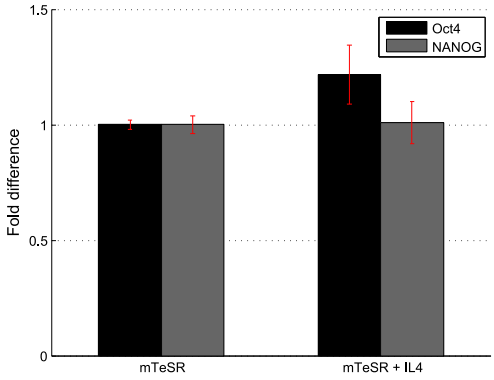

Figure 3.10: *Expression of the pluripotency transcription factors Oct-4 and Nanog as determined by real-time reverse-transcription PCR. GAPDH was used as endogenous control and the expression was normalised to expression in mTeSR.*

3.5 T8 in mTeSR differentiation assay

The T8 cell line was grown under selective pressure using a G418 resistance marker incorporated under control of the Oct-4 promoter. The antibiotic was removed from the growth media shortly before passaging cells into the assay. Figure 3.11 shows the typical morphology of a T8 colony and the expression of the green fluorescent EGFP before the assay was started.

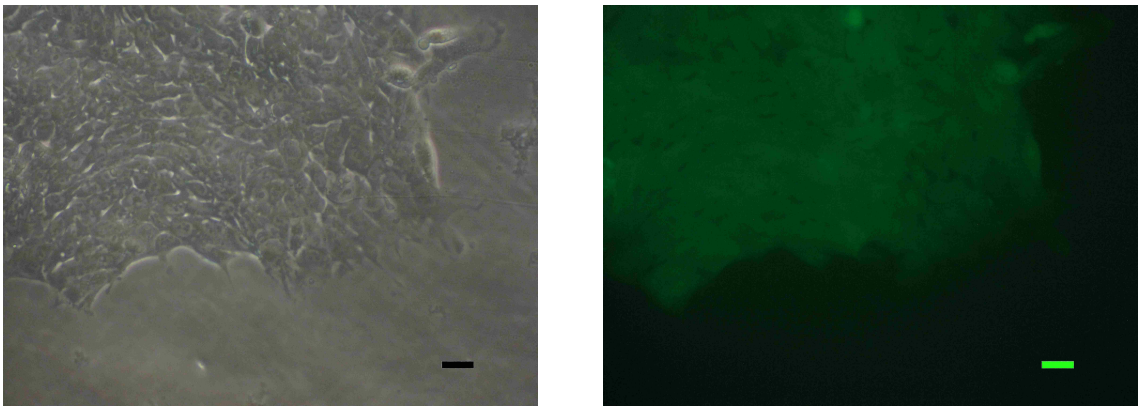

A B

Figure 3.11: *The expression of GFP by T8 cells at the beginning of experiments. A shows a phase contrast image of the colony that consist of almost only ES-like cells. B) shows the green fluorescence of the same area. All cells express the green fluorescent EGFP. Scale bar, 25 μm.*

Very few cells of non-ES like morphology were present in the T8 cells when G418 was removed from the media. Figure 3.12 shows cells during the experiment. Cells of non-ES like morphology can be seen as the flat dispersed cells outside a colony of ES-like cells. The expression of EGFP corresponds with cells of ES-like morphology.

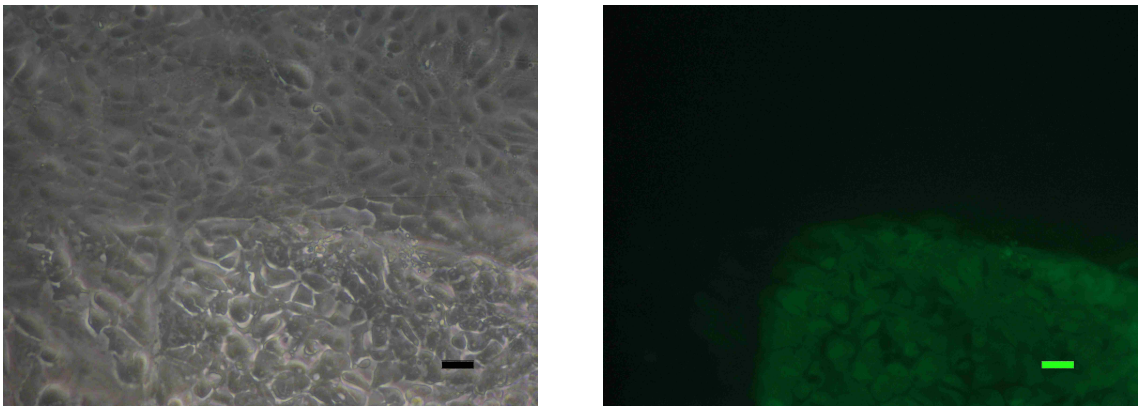

A B

Figure 3.12: *The expression of GFP by T8 cells during the differentiation assay. A shows a phase contrast image of the T8 cells that consist of two morphologies: A compact colony of ES-like cells and dispersed cells of non-ES like morphology. B shows the green fluorescence of the same area. The expression of EGFP by T8 cells correspond with ES like morphology. Scale bar, 25 μm.*

4 wells of each condition were removed and analysed every 24 hours starting just prior to the transition from mTeSR to the six different media. The cells were stained with the nuclear dye Hoechst stain, and the total blue and green fluorescence of each well was measured with an automated plate reader. The EGFP/Hoechst ratio was calculated for each well, abnormalities of more than 10% deviation from average of the 4 values of each condition was removed and the average of the remaining values was normalised with respect to the positive control. The ratio is plottet in Figure 3.13. No clear pattern could be observed.

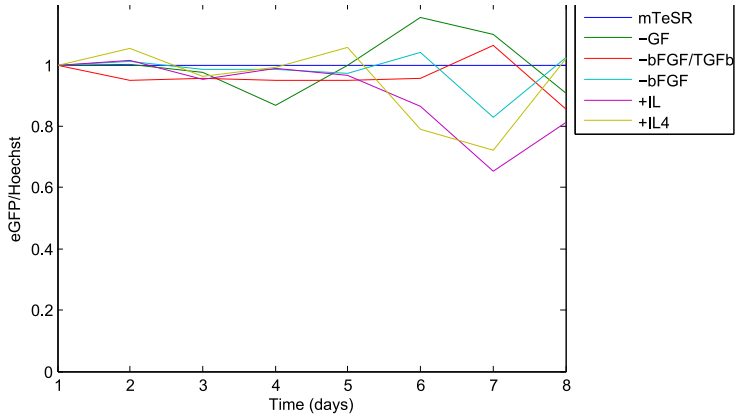

Figure 3.13: *Normalised ratio of EGFP/Hoechst signal from wells with T8 growing under different conditions. X-axis is days since the initial seeding of cells in mTeSR media. Different conditions were applied at day 1.*

The morphology of cells at the end of the first passage showed no difference between conditions, while different morphologies were observed during passage 2. Figure 3.14 shows the six different conditions at the end of passage two. Only ES like cells could be observed in the positive control, while the negative control area-wise consisted of half ES like cells and half non-ES like cells. The removal of TGFβ in the "-bFGF" sample showed no effect compared to the positive control at the end of passage two, but some differentiation was observed in the three samples without bFGF and TGFβ. The addition of IL4 seemed to decrease the amount of differentiation.

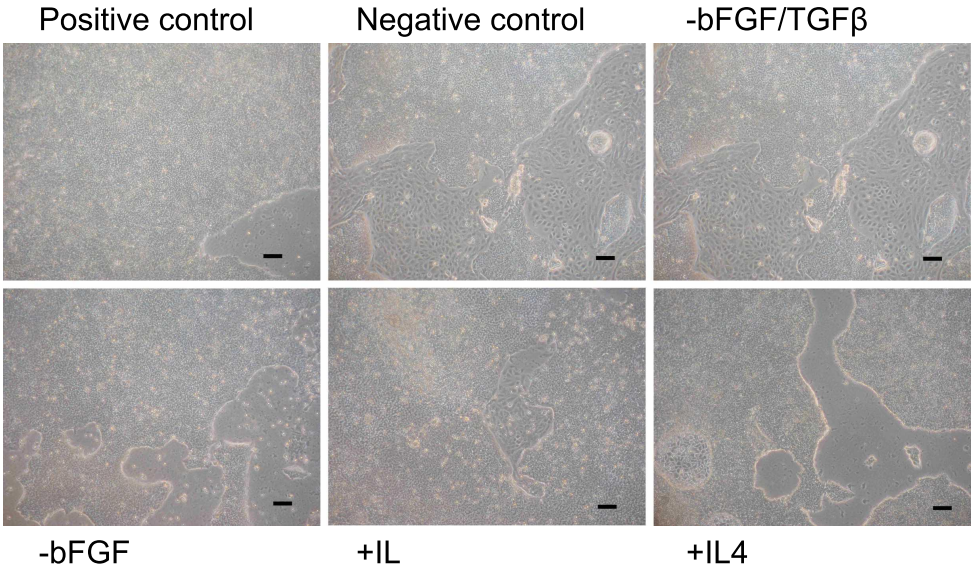

Figure 3.14: *Passage two of the T8 in mTeSR differentiation assay. Phase contrast images show the development of cell morphology of the six conditions described in Table 2.2. Considerable amounts of differentiation is evident in the negative control. Scale bar, 100 μm.*

Cell counting of EGFP positive cells was applied during the second passage. 4 wells of the 96 well plate of each condition were removed and analysed every 24 hours by a capture of green and blue fluorescence

images of 3 areas of each well and cells were counted as described in Appendix C. The ratio of EGFP positive cells to Hoechst stained cells during the passage is shown in Figure 3.15. Cell counting was performed from one day after passaging and for five days. Counting was not possible when the well reached a higher level of cell density. The EGFP/Hoechst ratio of the positive control is near one, while the negative control is significantly lower than the remaining conditions.

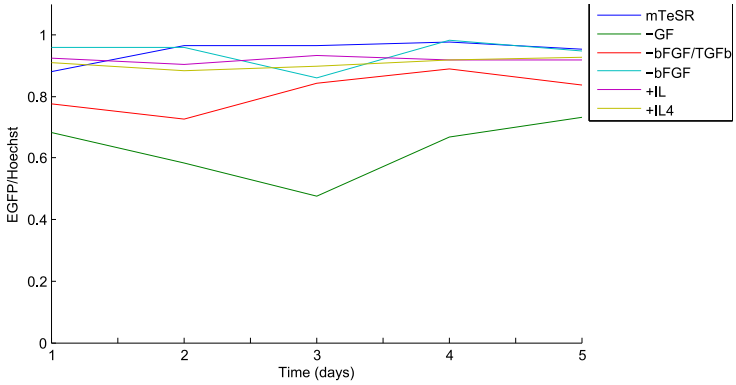

Figure 3.15: *Ratio of EGFP positive cells to Hoechst stained cells during passage two. X-axis is days since the passaging of cells.*

Figure 3.16 shows the morphology of cells at the end of passage four. The positive control showed only a neglectable level of differentiation, while the negative control and the cells added indolicidin now consisted of two distinct non-ES like morphologies. The addition of IL4 had significantly decreased the amount of cells of non-ES like morphology.

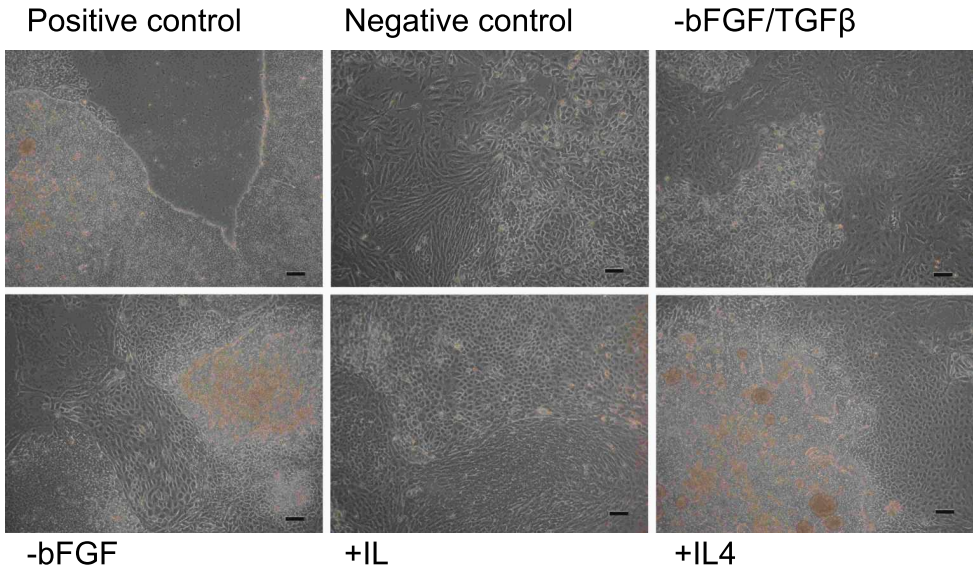

Figure 3.16: *Passage four of the T8 in mTeSR differentiation assay. Phase contrast images show the development of cell morphology of the six conditions described in Table 2.2. The positive control shows only ES like cells, while differentiation is evident in the five other conditions. Scale bar, 100* µm.

Real-time reverse-transcription PCR was performed on the isolated RNA from all six conditions. The

relative change in Oct-4 and Nanog expression compared to the positive control is given in Figure 3.17. No change was seen in the Oct-4 expression of the positive control, but more than a 60% drop was seen in all samples except the "-bFGF" that was added TGFβ. The expression of Oct-4 was higher in the sample added IL4 than in the "-bFGF/TGFβ" sample, which otherwise contained the same media. The expression of Nanog remained constant in the positive control, but a characteristic drop in the second passage and then increase to the fourth passage was evident for the other five conditions.

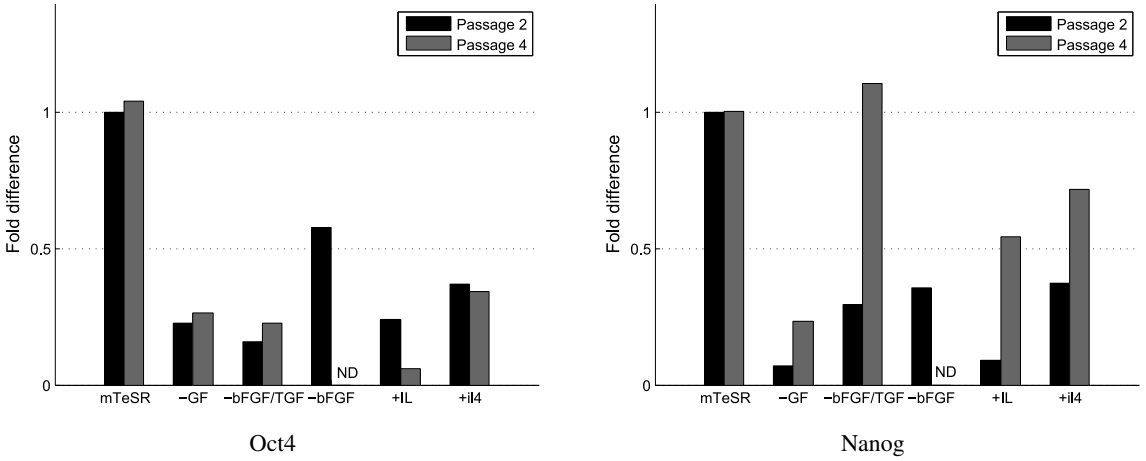

Figure 3.17: *Expression of the pluripotency transcription factors Oct-4 and Nanog as determined by real-time reverse-transcription PCR. GAPDH was used as endogenous control and the expression was normalised to the positive control at passage 2.*

3.6 RH1 in E8 differentiation assay

RH1 cells were gradually transitioned from mTeSR to the chemically defined E8 media over a five passage period. RH1 cells transitioned to E8 showed signs of stress and around 20% of the cells were differentiating. Figure 3.18 shows the general morphology of cells before passaging at the beginning of the assay.

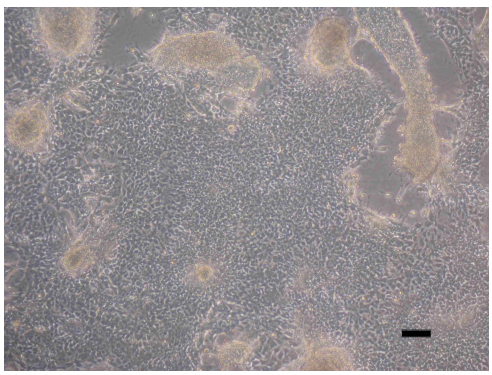

Figure 3.18: *RH1 cells growing on E8 media. The cells were transitioned from mTeSR to E8 over a five passage period and showed an increased degree of differential stress compared to the counterpart growing on mTeSR. Scale bar, 100 μm.*

The effect of 50µg/mL IL4 or 20 µg/mL IL was tested by 5 days growth and analysed by comparison with cells growing on E8. Four biological repilicates were used for all conditions. 24 hours of incubation with indolicidin added to E8 medium had a drastic effect, as illustrated by the phase contrast images of the four conditions in Figure 3.19. A clear loss of cells was observed in all wells where indolicidin was added, while cell growing on E8, E8 + IL4 or E6 showed similar growth.

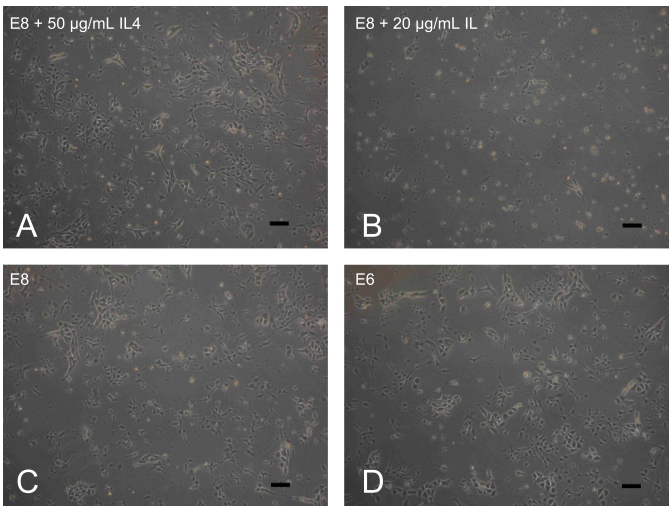

Figure 3.19: *RH1 cells after one days growth in the media: (A) E8 + 50µg/mL IL4, (B) E8 + 20 µg/mL IL, (C) E8 and (D) E6. The addition of indolicidin has caused a clear loss of cells. Scale bar, 100 µm.*

The effect of 5 days growth is shown in Figure 3.20. Indolicidin-4 had a diminishing effect on the cell growth, leaving the well at less than 80% confluency, while the E8 control was at 100%. The negative E6 control showed the same morphology as E8 and no living cells could was left in the wells where indolicidin was added.

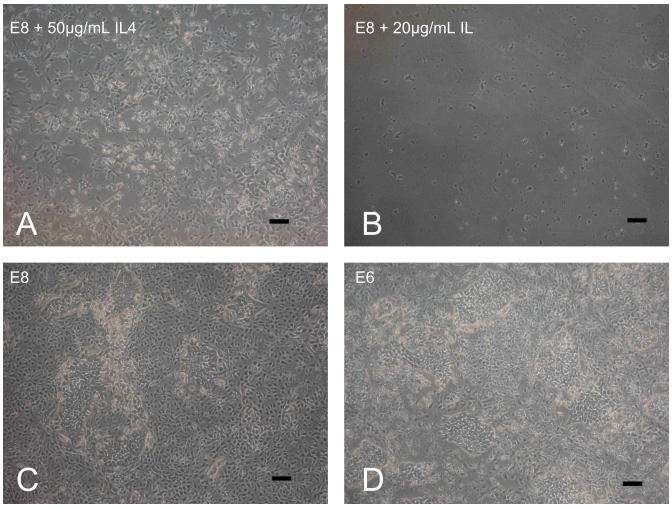

Figure 3.20: *RH1 cells after one 5 days growth in the medias: (A) E8 + 50µg/mL IL4, (B) E8 + 20 µg/mL IL, (C) E8 and (D) E6. The addition of indolicidin has caused a clear loss of cells, while the addition of IL4 had a diminshing effect on the cell growth. Scale bar, 100 µm.*

The expression of the pluripotency transcription factor Nanog was estimated using real-time reverse-transcription PCR. The relative expression of Nanog was compared to RH1 cells growing on mTeSR, these cells were of the same passage as the ones transitioned to E8 and had been prepared as a control. Figure shows the Nanog expression normalised to GAPDH and relative to mTeSR cells. The transition to E8 caused the expression of Nanog to drop to 85% of what was observed for the control on mTeSR, while the 5 days growth on E6 increased the expression to 95%. Fewer cells were isolated from the wells added IL4 and the expression of Nanog in these cells dropped to 48% of the mTeSR counterpart. No cells could be isolated from the wells added indolicidin.

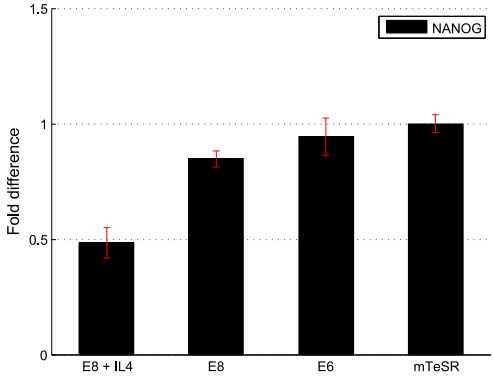

Figure 3.21: *Expression of the pluripotency transcription factor Nanog as determined by real-time reverse-transcription PCR. GAPDH was used as endogenous control and the expression was normalised to expression in mTeSR.*

3.7 Fragmentation of DNA

3.7.1 Fragmentation by Sonication

Sonication was used to fragment DNA isolated from human dermal fibroblast cells and from RH1 embryonic stem cells. Figure 3.22 shows the effect of increasing sonication time on HDF DNA as observed by gel electrophoresis. Unprocessed DNA was loaded in well B and the migration length corresponds to the main part of DNA being larger than 10,000 bp, and the remaining part distributed somewhat evenly at all sizes down to 250 bp. DNA fragmented by 1 minute sonication was loaded in well C, and the following wells show the effect of a one minut increase in sonication time up til 8 minutes, while a sample of 20 minutes sonication is loaded in well K. A band of DNA larger than 10,000 bp was observed from the unprocessed DNA and this band gradually decreased in size until it was completely degraded at 5 minutes sonication.

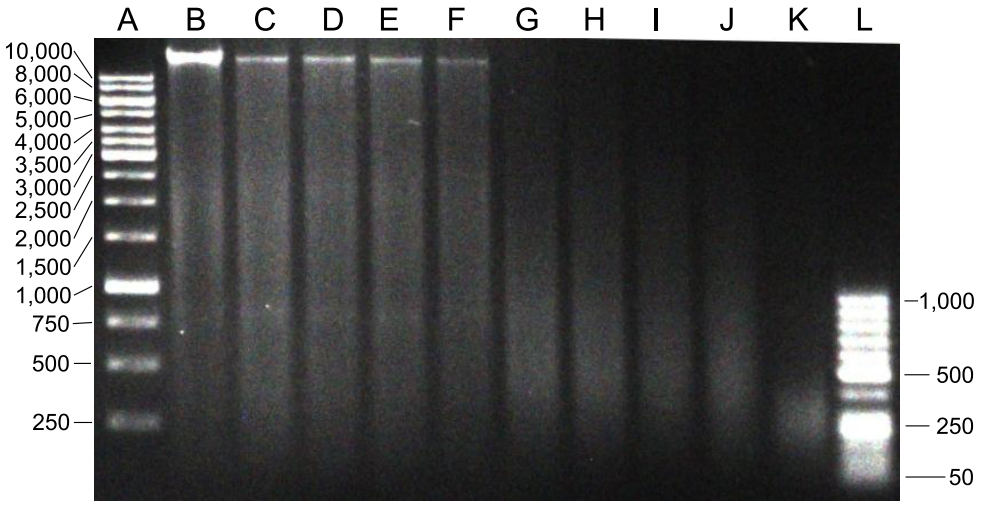

Figure 3.22: *Gel electrophoresis of HDF DNA fragmented by sonication. 1% agarose gel. B: unprocessed DNA, C: 1 D: 2, E: 3, F: 4, G: 5, H: 6, I: 7, J: 8 and K: 20 minute sonication.*

Brightness distribution of the gel is shown in Figure 3.23. The color intensity along the migration length of each well is plotted in the figure. The background signal has been subtracted and the mean of each sample is shown with a vertical line. The position of ladder bands is marked on the x-axis. The brightness along 3 lines of each column was measured using the RGB Profile Plot of ImageJ and the mean with a 20 point moving average plotted in MATLAB. The mean of the migration length was calculated as:

$$\sum \frac{x * i}{i_t}, \tag{3.1}$$

where x is the migration length from the well, i is the color intensity at said migration length and i_t is the total intensity from the column. It can be observed that the DNA size decrease with increasing sonication time, though in a somewhat erratic pattern.

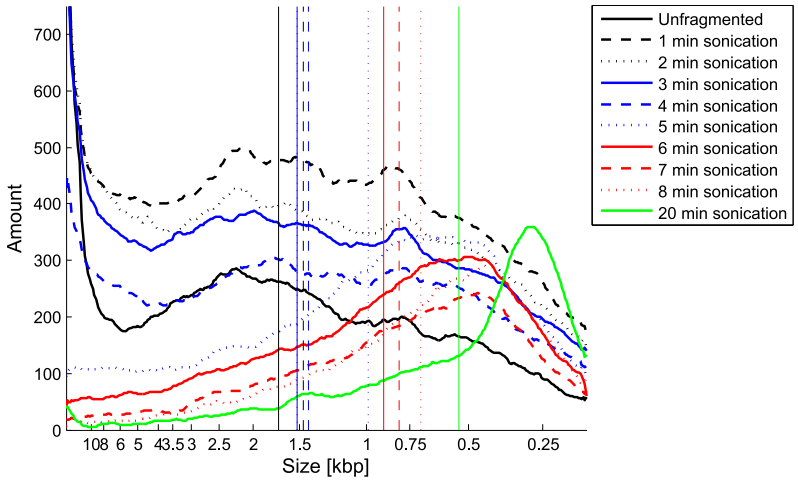

Figure 3.23: *Size distribution of HDF DNA at increasing sonication time. The brightness distribution along each column of Figure 3.22 is given with a different style and the mean migration length is plotted with a vertical line. The DNA size decrease with increasing sonication time.*

The effect of sonication on RH1 DNA as observed by gel electrophoresis is shown in Figure 3.24. The unprocessed DNA was loaded in well B, and the migration length corresponds to almost the entire DNA being larger than 10,000 bp. The following wells show the effect of increasing sonication times from 1 to 8 minutes and well K shows the effect of 20 minutes sonication. An increasing migration length is observed as the sonication time is increased.

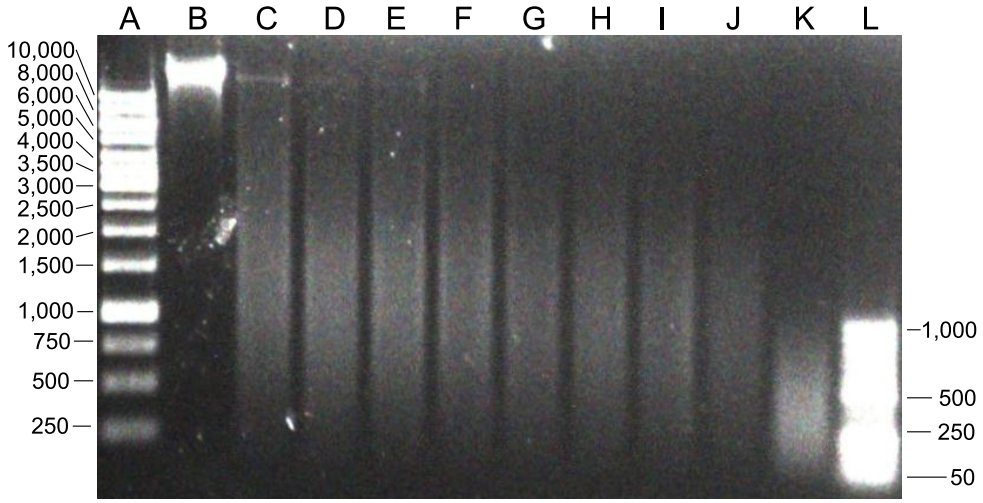

Figure 3.24: *Gel electrophoresis of RH1 DNA fragmented by sonication. 1% agarose gel. B: unprocessed DNA, C: 1 D: 2, E: 3, F: 4, G: 5, H: 6, I: 7, J: 8 and K: 20 minute sonication.*

Brightness distribution of the gel is shown in Figure 3.25. The color intensity along the migration length of each well is plotted in the figure. The DNA size decrease with increasing sonication time. The main fragmentation occurs during the first minute and then at a decreasing rate at longer sonication times. A bell curve distribution can be observed at all sonication times with a Gaussian like distribution obtained after 20 minutes sonication.

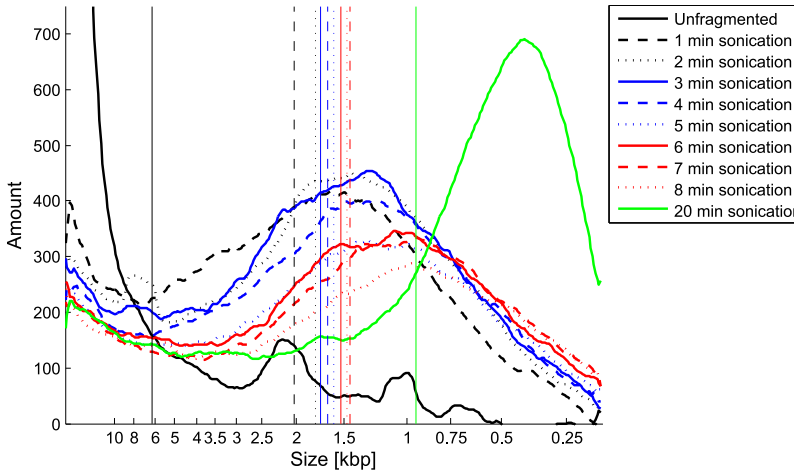

Figure 3.25: *Size distribution of RH1 DNA at increasing sonication time. The brightness distribution along each column of Figure 3.24 is given with a different style and the migration length is plotted with a vertical line. The DNA size decrease with increasing sonication time.*

Gel electrophoresis of DNA subjected to prolonged sonication time (60 min+) is shown in Figure 3.26. A distribution around 150 bp was obtained for both HDF and RH1 DNA. Further sonication did not decrease the DNA size.

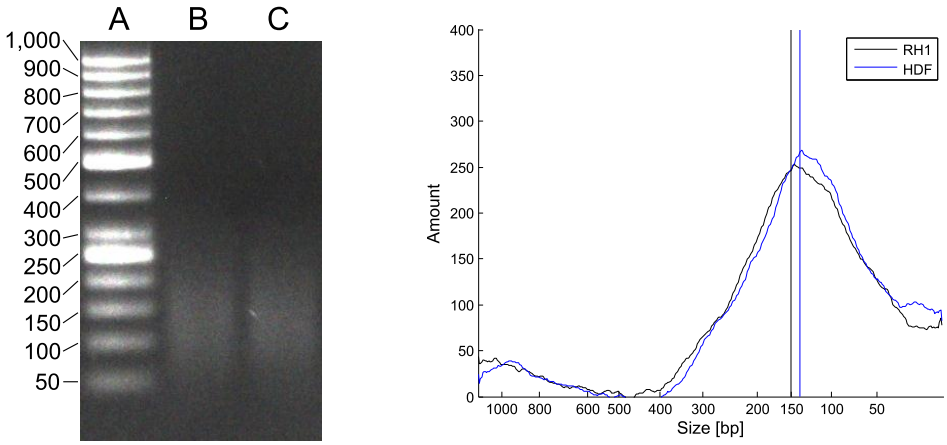

A B

Figure 3.26: *Gel electrophoresis of HDF and RH1 DNA fragmented by 60 minutes sonication. A: 2% agarose gel. HDF DNA loaded in well B and RH1 DNA in well C. B: Brightness distribution along the two columns.*

3.7.2 Fragmentation by Restriction Enzyme Digestion

Gel electrophoresis of HDF and RH1 DNA digested using the restriction endonucleases EcoRI and XhoI is shown in Figure 3.27. Both samples showed a distribution of sizes from approximately 750 bp to larger than 10,000 bp. The main part of DNA had a size of 2,000 to 10,000 bp.

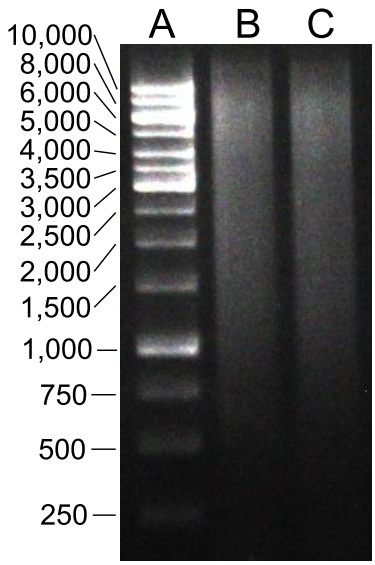

Figure 3.27: *Gel electrophoresis of HDF and RH1 DNA digested with restriction endonucleases EcoRI and XhoI. 1% agarose gel. B: HDF DNA, C: RH1 DNA.*

3.8 High-resolution Atomic Force Microscopy

Atomic force microscopy was performed on unprocessed DNA. Figure 3.28 shows the topograhy of HDF DNA with no fragmentation attached to an APTMS coated mica surface. The scan size of 4µm x 4µm in (A) shows a distribution of structures approximately 200 nm in width and less that 2 nm in height. The 1µm x 1µm scan size in (B) reveals that the structures consist of two components: Long curled strands of several hundred nanometer length and aggregates of smaller strands. The height of single strands was 0.6 to 1.0 nm.

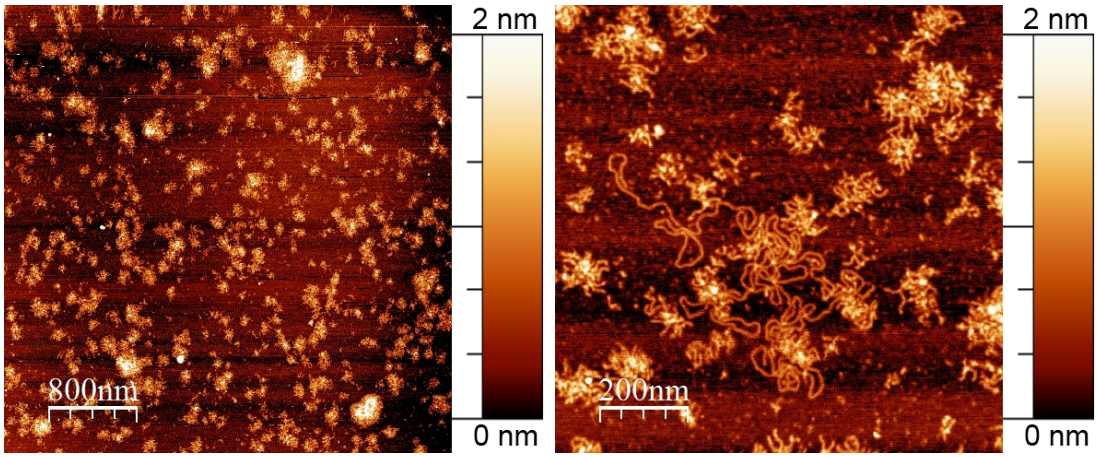

Figure 3.28: *AFM topography of HDF DNA immobilised on an APTMS-mica surface. (A) 4µm x 4µm scan size, (B) 1µm x 1µm scan size. The DNA was not fragmented before immobilisation. 40 µl of 1.25 µg/mL DNA was deposited.*

RH1 DNA was likewise immobilised on an APTMS-mica surface and imaged using AFM. Figure 4.3 shows the topograhy of RH1 DNA with no fragmentation. Long curled strands and few shorter strands were observed, but unlike the HDF DNA sample, no aggregates of short strands were observed, and the majority of observed structure was composed of several hundred nanometer length strands. The height of single strands was 0.5 to 0.9 nm.

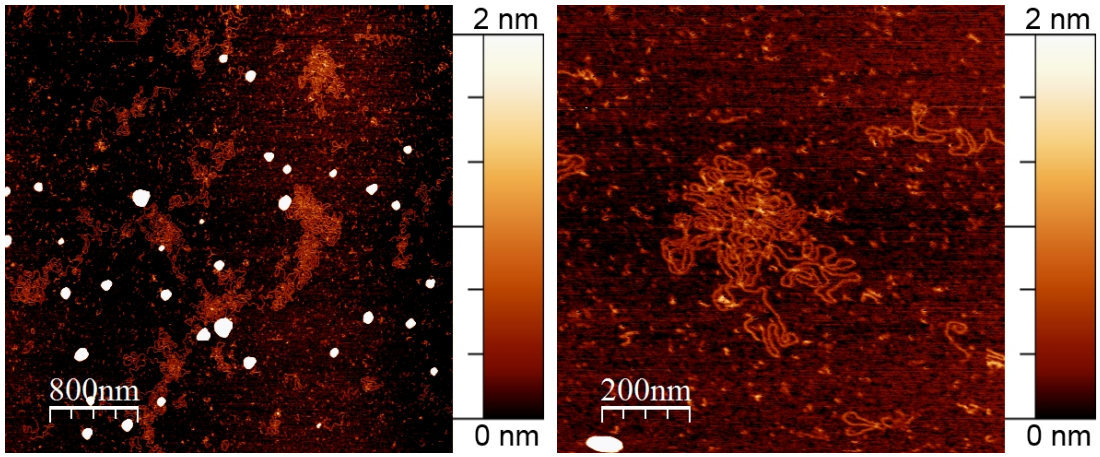

A B

Figure 3.29: *AFM topography of RH1 DNA immobilised on an APTMS-mica surface. (A) 4μm x 4μm scan size, (B) 1μm x 1μm scan size. The DNA was not fragmented before immobilisation. 40 μl of 1.25 μg/mL DNA was deposited.*

DNA fragmented by sonication was attached to APTMS-mica surfaces. Examples of the AFM topograhy obtained for sonication of HDF DNA is shown in Figure 3.30. The sample in (A) was sonicated for 3 minutes and the sample in (B) for 6 minutes. Strand structures with length of 50 to few hundred nanometers were observed in both samples. The structure varied in height from 0.4 to 0.9 nm.

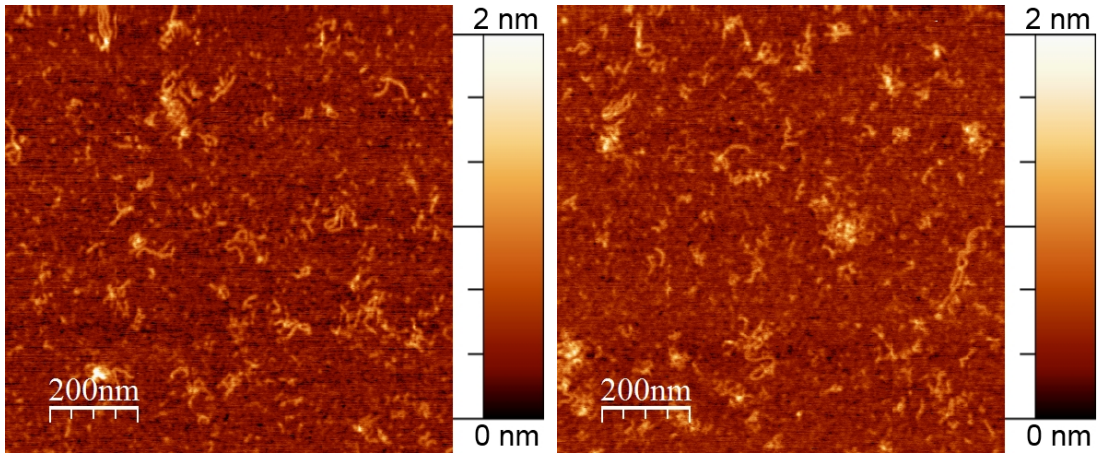

A B

Figure 3.30: *AFM topography of HDF DNA immobilised on an APTMS-mica surface. A: Fragmented by 3 minutes sonication, and B: 6 minutes. Gel electrophoresis of the same samples are shown in Figure 3.22. 40 μl of 1.0 μg/mL DNA was deposited on both samples. 1μm x 1μm scan size.*

AFM topograhy of RH1 DNA fragmented by 3 minutes sonication is shown in Figure 3.31 (A) and 8 minutes sonication in (B). Strand structures with length of 50 to 1,000 nanometers was observed in both samples. The structure varied in height from 0.6 to 1.0 nm

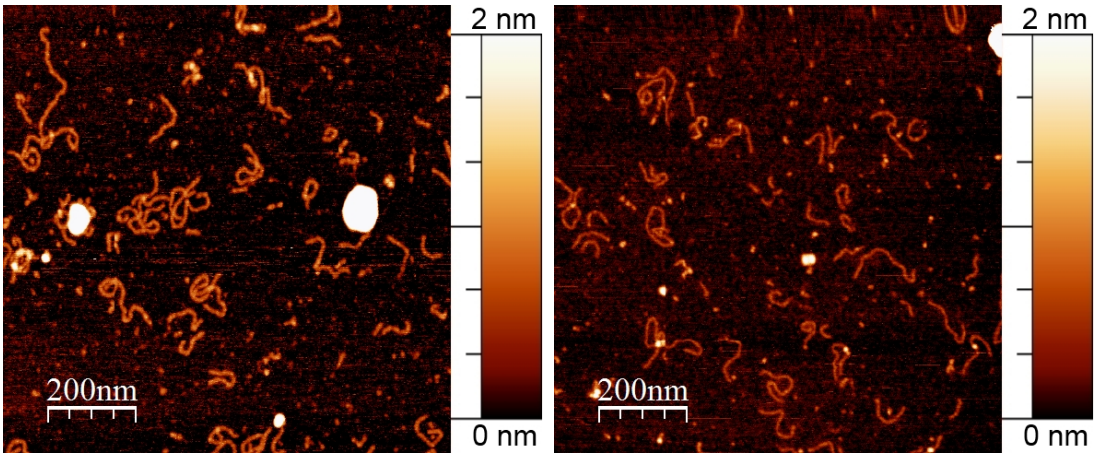

A B

Figure 3.31: *AFM topography of RH1 DNA immobilised on an APTMS-mica surface. A: Fragmented by 3 minutes sonication, and B: 8 minutes. Gel electrophoresis of the same samples are shown in Figure 3.24. 40 µl of 1.0 µg/mL DNA was deposited. 1µm x 1µm scan size.*

The size distribution of the strands observed from 3 and 8 minutes sonication of RH1 DNA was determined from a total area of 4µm x 4µm. The same conditions as used for the above AFM scan was applied. The length of all strands longer than 50 nm was measured and the distribution in 100 nm intervals is shown in Figure 3.32. The 50 to 100 nm interval has been given the same width as those of a hundred nm for visual effect. A displacement towards smaller sizes is evident from 3 to 8 minutes sonications. The mean size (calculated using the measured lengths) was 280 nm for 3 minutes sonication and 245 nm for 8 minutes sonication.

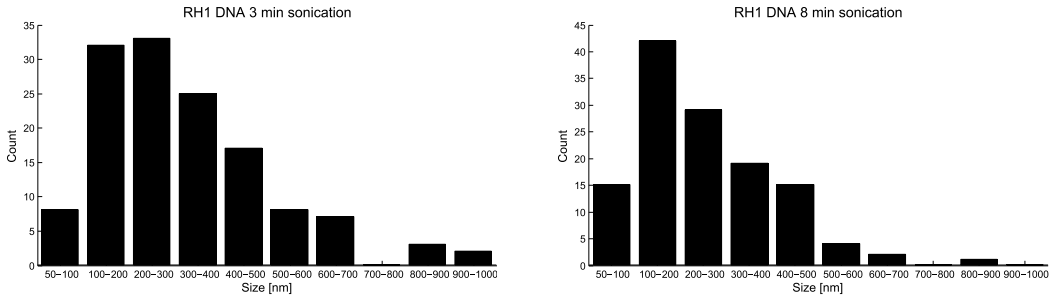

A B

Figure 3.32: *Size distribution of strand structures observed in AFM. A: RH1 DNA fragmented by 3 minutes sonication. B: RH1 DNA fragmented by 8 minutes sonication. The length of all strands longer than 50 nm was measured in a total area of 4µm x 4µm.*

Figure 3.33 shows a typical AFM topography obtained from DNA fragmented by restriction endonuclease digestion. Strand structures with a wide distribution of lengths was observed with the smallest at 100 nanometers and the largest several thousand nanometers. A lot of smaller and larger "dirt" was also observed.

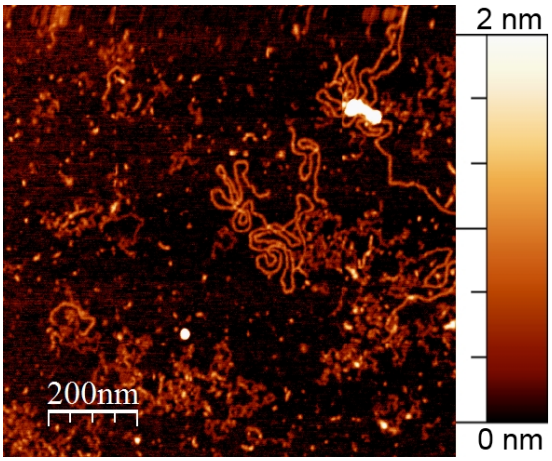

Figure 3.33: *AFM topography of RH1 DNA immobilised on an APTMS-mica surface. The DNA is digested with restriction endonucleases EcoRI and XhoI. Gel electrophoresis of the same samples are shown in Figure 3.27. 40 µl of 1.0 µg/mL DNA was deposited. 1µm x 1µm scan size.*

3.8.1 Binding of IL4 to DNA

IL4 was added to a droplet of the linearised plasmid pUC19 after 5 minutes incubation on the APTMS-mica surface. The observed result depended on the concentration of IL4 added. Figure 3.34 shows the AFM topography obtained when 10 µL ammonium acetate buffer with no IL4 was mixed with the DNA. The average height of the strand structures was 6 to 8 Å.

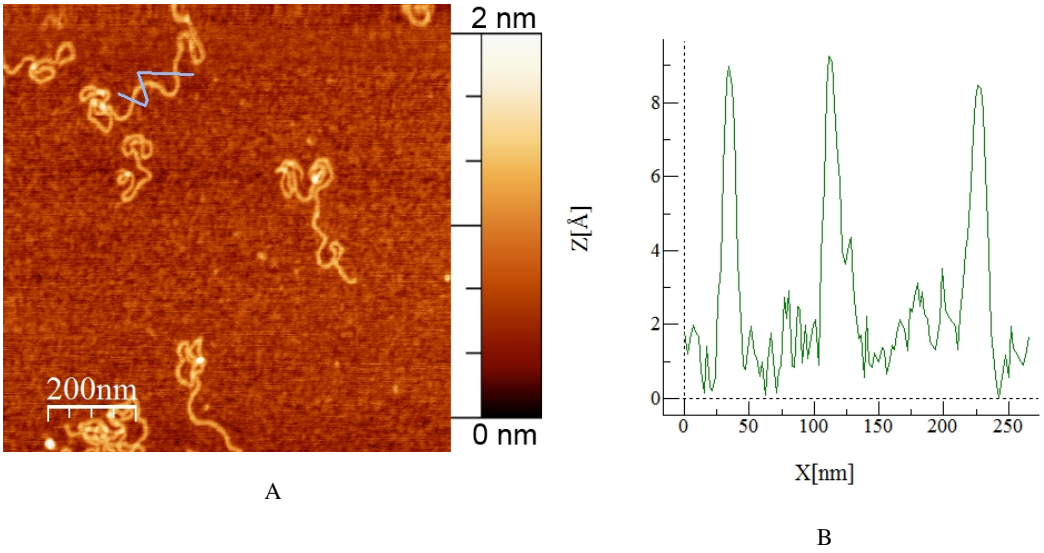

Figure 3.34: *AFM topography of pUC19 DNA immobilised on an APTMS-mica surface. A: 1µm x 1µm scan of the linearised plasmid. B: Height profiles of the blue line on the topography image. The average height of the strand structures was 6 to 8 Å. 40 µl of 0.5 µg/mL DNA was deposited.*

10 µL 50 µg/mL IL4 was added to 40 µl of 0.5 µg/mL pUC19 DNA for a final concentration of 6.2 µM IL4 and 0.6 µM base pairs DNA. Figure 3.35 shows the AFM topography obtained. The average height

of the strand structures was 1 to 1.2 nanometer.

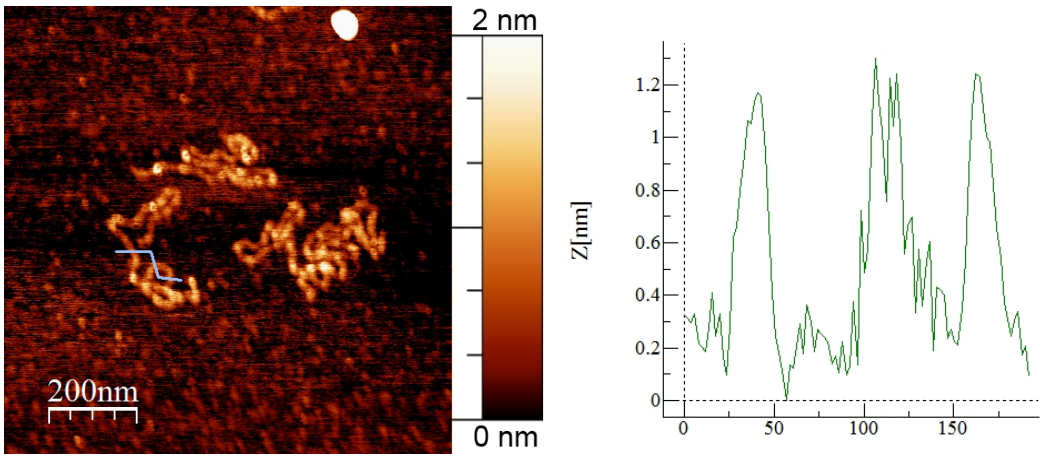

A

B

Figure 3.35: *AFM topography of pUC19 DNA, added a final concentration of 10 µg/mL IL4, immobilised on an APTMS-mica surface. A: 1µm x 1µm scan. B: Height profiles of the blue line on the topography image. The average height of the strand structures was 1 to 1.2 nm. 40 µl of 0.5 µg/mL DNA was deposited.*

10 µL 1 mg/mL IL4 was added to 40 µl of 0.5 µg/mL pUC19 DNA for a final concentration of 124 µM IL4 and 0.6 µM base pairs DNA. Figure 3.36 shows the AFM topography obtained. The general surface topography varied 0.5 nm in height, and strand structures were observed with a total height of 1.4 to 2.0 nm.

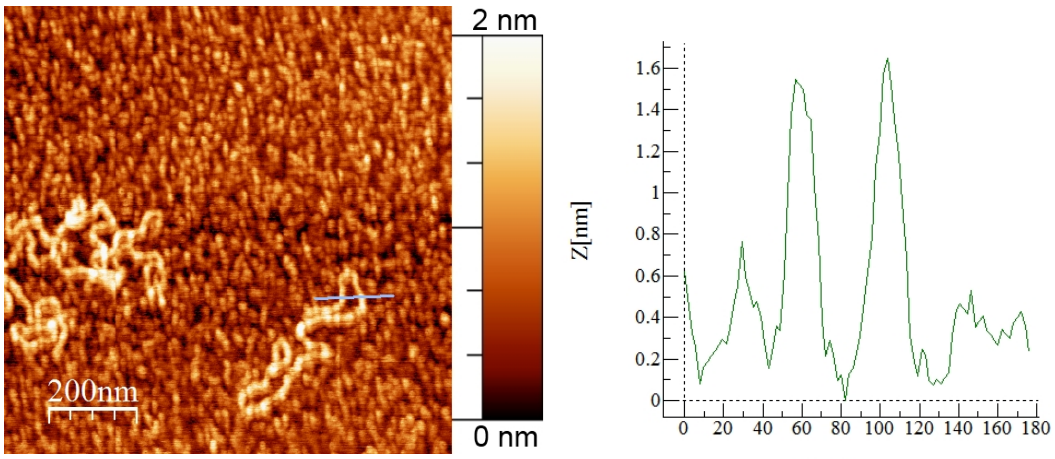

A

B

Figure 3.36: *AFM topography of pUC19 DNA, added a final concentration of 200 µg/mL IL4, immobilised on an APTMS-mica surface. A: 1µm x 1µm scan. B: Height profiles of the blue line on the topography image. The average height of the strand structures was 1.4 to 2.0 nm. 40 µl of 0.5 µg/mL DNA was deposited.*

The addition of 10 µL 50 µg/mL IL4 to RH1 DNA digested by 8 minutes sonication produced afm topographies as the one observed in Figure 3.37. The final concentrations are 6.2 µM IL4 and 1.2 µM base pairs DNA. Strand structures with an average height of 0.8 to 1.1 nm were observed.

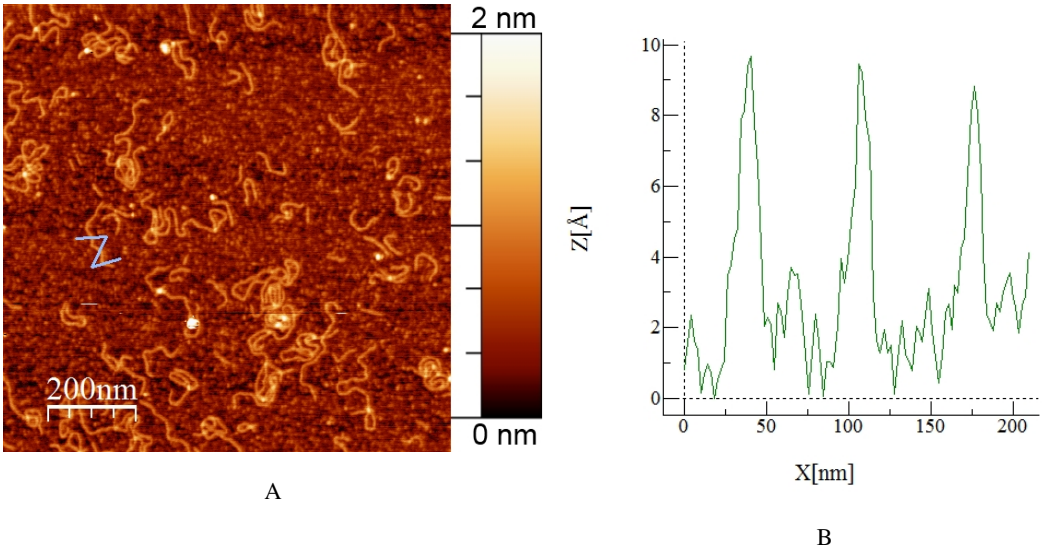

Figure 3.37: *AFM topography of RH1 DNA fragmented by 8 minutes sonication, added a final concentration of 10 µg/mL IL4, immobilised on an APTMS-mica surface. A: 1µm x 1µm scan. B: Height profiles of the blue line on the topography image. The average height of the strand structures was 0.8-1.1 nm. 40 µl of 1.0 µg/mL DNA was deposited.*

10 µL 50 µg/mL IL4 was added to 40 µl of 1.0 µg/mL HDF DNA digested by 8 minutes sonication for a final concentration of 6.2 µM IL4 and 1.2 µM base pairs DNA. Figure 3.38 shows the AFM topography obtained. Strand structures with an average height 0.9 to 1.2 nm were observed. The DNA had been treated with RNAse A before the experiment (see Section 4.11 for details).

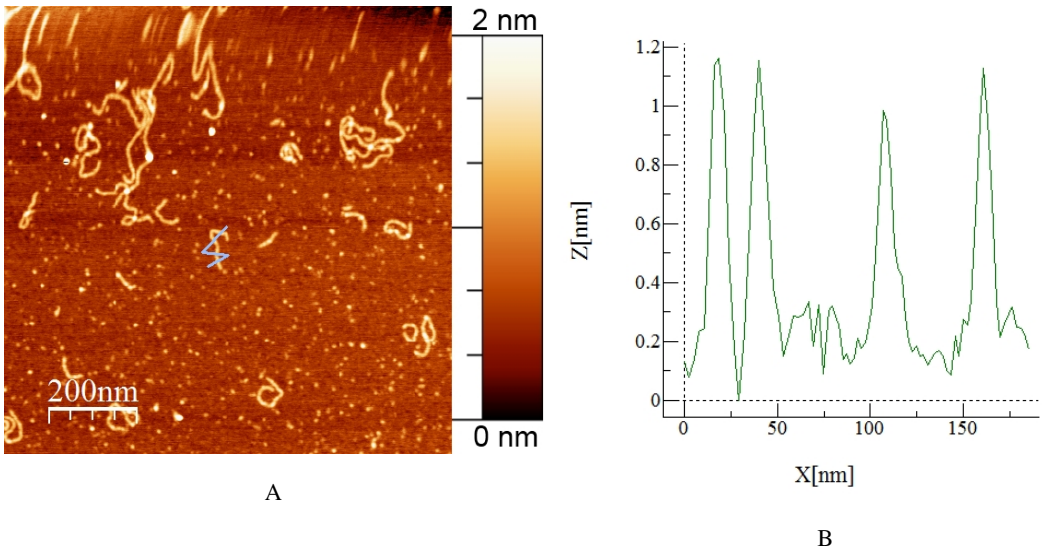

Figure 3.38: *AFM topography of HDF DNA fragmented by 8 minutes sonication, added a final concentration of 10 µg/mL IL4, immobilised on an APTMS-mica surface. A: 1µm x 1µm scan. B: Height profiles of the blue line on the topography image. The average height of the strand structures was 0.9-1.2 nm. 40 µl of 1.0 µg/mL DNA was deposited.*

4 Discussion

4.1 Peptide synthesis and purification

The success of each deprotection and coupling in the synthesis of the peptides IL4 and IL4-RWT was confirmed using the ninhydrin[83] or chloranil test[84]. The ninhydrin molecule reacts with primary amines in a condensation forming a chromophore if >1% of the amines are deprotected. This gives the possibility of up to 12% and 14% peptide of unwanted sequence for IL4 and IL4-RWT respectively. Deprotection was always performed twice as the ninhydrin test shows a positive result at >1% deprotection, and as such can not be used to ensure proper deprotection. The design of IL4-RWT included the coupling of an amino hexanoic acid between the original IL4 structure and the rhodamine water tracer fluorophore. This was done to minimise the effect of placing the dye next to the hydrophobic N-terminus that, according to Marchand *et al*, might be important for the binding to DNA[11].

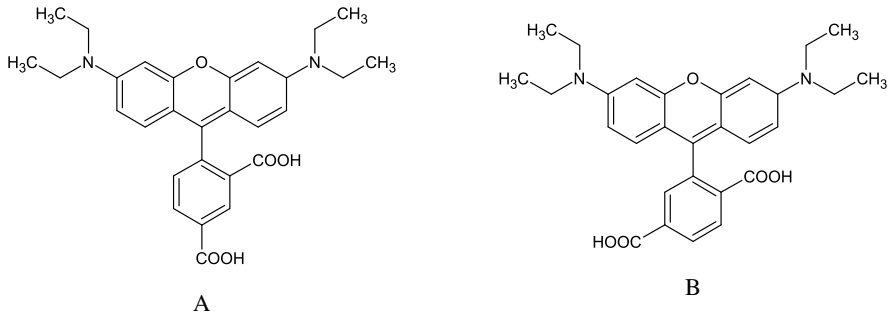

Figure 4.1: *The molecular structure of the dye rhodamine water tracer. The dye has two isomers differing in the positioning of the carboxylate groups on the phenyl: Meta (A) and para (B).*

RP-HPLC analysis of the IL4 synthesis product showed a pure product eluted at approximately 38 % ACN. 214 nm absorption detects the peptide bond and 280 nm detects the amino acids Tyr, Trp (to some extent Phe and disulfide bonds)[91] of which only tryptophan was used in the synthesis. Few minor peaks were detected at both 214 and 280 nm corresponding to products lacking amino acids or otherwise resulting from a defective synthesis. Mass spectrometry showed an isotope distrbution with the first peak at a m/z of 1614.2 corresponding to the monoisotopic mass of IL4 + H^+ of 1614.073 g/mol, verifying that the isolated peptide was indeed IL4.

IL4-RWT was less pure than IL4 and produced two peaks corresponding to the two isomers[89]. Separation of the peaks was not possible, but MS showed only one signal of 2198. The monoisotopic mass of

IL4-RWT was calculated as 2197.35 g/mol confirming that the isolated product was IL4-RWT. Concentration measurements were based on 550 nm absorption using an extinction coefficient of 87,000[92].

4.2 Choice of Cell Culture System

Cell culture work was performed at the MRC Centre for Regenerative Medicine, University of Edinburgh, working with a group focused on pluripotent cell translation[93]. The standard system for embryonic stem cell growth was the media mTeSR®1 and the support Matrigel™, described in Section 1.1.1. The cytotoxic concentration of the peptides was determined in mTeSR followed by a short term assay using RH1 cells to test the effect of IL4 on stem cell pluripotency. The effect was then tested over several passages using the T8 cell line. The complete mTeSR is a very rich media capable of supporting the growth of embryonic stem cells without loss of differentiation potential over extended periods, and the simpler E8 media was ultimately used to test the effect of the peptides on embryonic stem cells.

4.3 Cultivation of Cells

The human embryonic stem cell lines RH1 and T8 and a human dermal fibroblast cell line were utilised in the project. RH1 cells introduced to experiments were at passage 72 to 80, T8 cells at passage 88 to 94 and HDF at passage 6 to 9. Both stem cell lines had been routinely used in differentiation assays and tested for expression of stem cell related surface markers and transcription factors. Mycoplasma testing was performed routinely. The routinely maintenance of RH1 cells rarely required the used of selection pressure, as described in Section 2.2, but a small amount of spontaneous differentiation occurred, as was expected. The T8 cell line required no selection pressure due to the G418 resistance marker incorporated under control of the Oct-4 promoter. The expression of Oct-4 is a key regulator of pluripotency[94], and differentiated cells were expected to lose the expression of Oct-4 and become susceptible to G418. Spontaneous differentiation of T8 was however confirmed when G418 was removed from the media.

Figure 4.2 shows the generally observed morphology of healthy RH1 cells (A) next to WA16 cells (B) maintained in TeSR1 as published in the original article describing the media[25]. The single colony in (B) can be seen as representative of the ideal morphology of ES cells: Compact cells of approximately 14 μm[95] in well defined colonies.

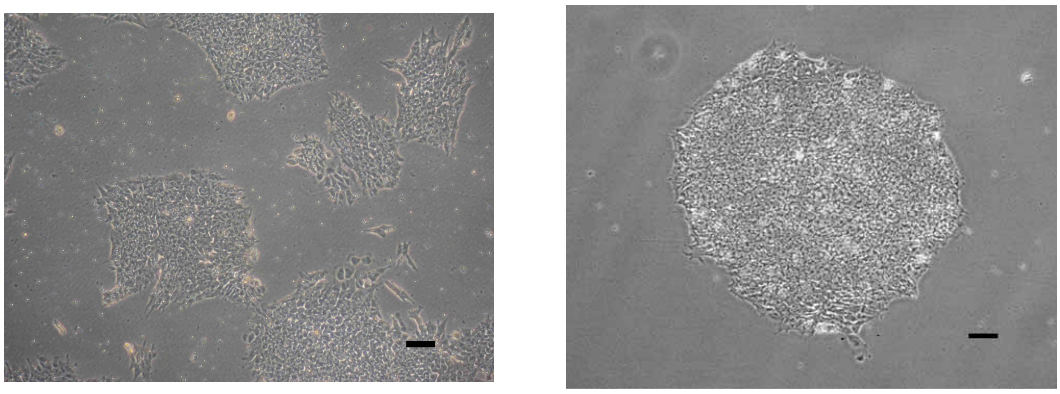

A B

Figure 4.2: *Phase contrast image of healthy hES cells. (A): RH1 cells during routine maintenance during the project. (B): WA16 cells maintained in mTeSR as published by Ludwig et al[25]. Both images were obtained by phase contrast microscopy using 4 x magnification. Scale bar, 100 μm.*

4.4 Cell Viability Assay

A cell viability assay was designed based on the CellTiter-Blue™ Cell Viability Assay[87]. The CellTiter-Blue assay uses the indicator dye resazurin to measure the metabolic capacity of cells as a direct indicator of cell viability. Viable cells retain the ability to reduce resazurin into the highly fluorescent resorufin and the fluorescent signal is, under optimal conditions, proportional to the number of viable cells. The amount of cells seeded into every well was adjusted low enough to ensure that confluency was not reached within 8 days, and high enough to minimise dissociation-induced apoptosis. The cells were passaged using trypsin that hydrolyse adhesion proteins in cell-cell and cell-matrix interactions creating a single cell suspension. Dissociated human embryonic stem have a poor survival rate and a ROCK inhibitor was added to ensure their survival upon passaging[96]. 10,000 cells were placed in a flat well with a surface area of 0.32 cm^2 yielding a density of 31,250 cells/cm^2. The density was observed to be high enough that no significant cell loss was detected upon removal of ROCK inhibitor, and confluency was normally not reached within the 8 days of the assay.

Indolicidin was cytotoxic to embryonic stem cells at $\geq$ 100 μg/mL, which is significantly higher than for the bacteria *E. coli* (16 μg/mL[97], 5 μg/mL[50]) and in the range of what has been observed for red blood cells (70 μg/mL[50]). Sub-cytotoxic concentrations could not be determined, but no cytotoxic effect was observed at $\leq$ 50 μg/mL. Indolicidin-4 was cytotoxic to embryonic stem cells at $\geq$ 333 μg/mL, also significantly higher than for *E. coli* (15 μg/mL[50]). The substitution of four tryptophan with leucine made the molecule less toxic as was expected. The addition of amino hexanoic acid and rhodamine WT to the N-terminus of IL4 increased the toxic effect of the peptide to cytotoxicity at $\geq$ 100 μg/mL.

4.5 Cellular uptake of IL4-RWT

Specific short cationic peptides such as the Tat 48–60 (GRKKRRQRRRPP) and R9 (RRRRRRRRR) possess cell-penetrating properties[98] making them capable of passing the membrane of most mammalian cells, and in particular stem cells[99]. Falla *et al* reported indolicidin to cross the outer membrane of *Escherichia coli* via the self-promoted uptake pathway[97], but no such studies have been performed for indolicidin-4. The high structural similarity to indolicidin and to the Tat and R9 sequences indicated that IL4 might possess the same cell-penetrating properties, and a fluorophore was coupled to test this hypothesis. The cytotoxic concentration of the new peptide IL4-RWT was between 50 and 100 μg/mL, and a concentration of 5 μg/mL was chosen to test the cell uptake. Confocal laser scanning microscopy showed single cells with a uniform distribution of peptide in the entire cell, but also concentration of peptide into smaller inclusions. The smaller inclusions corresponds with uptake through endocytosis, a process by which cells absorb molecules by engulfing them in vesicles.

Flow cytometry was performed to evaluate a larger number of cells. The cells were washed with PBS and incubated in Trypsin to remove any membrane-bound peptide, and a test was made by adding 0.4% trypan blue to the cells before flow cytometric analysis. This concentration of trypan blue quenched most fluorescence from IL4-RWT in solution, but no reduction of fluorescence was observed during flow cytometry. The correlation between cell uptake of IL4-RWT and incubation time is shown in Figure 3.8. A linear correlation was observed within the first 2 hours, and the maximum uptake was not obtained before 12 hours. The slow uptake indicates that the peptide is not trapped at the surface, but indeed enters the cells. The linear increase within the first 2 hours matches the results of Yukawa *et al.* with Tat and R8[99], which indicates an endocytosis related pathway.

Uptake in the nucleus could not be confirmed and the access to DNA was therefore not certain. The nuclear membrane allows free diffusion of most molecules smaller than 10 nm in diameter, but some molecules are restricted, even though they, as IL4, are far smaller than the 10 nm[70]. Small nuclear localization sequences exist, and the coupling of e.g. the nuclear localization sequence of the transcription factor NF-kB could have facilitated uptake in the cell nucleus[100,101], and thereby ensured the acces of IL4 to DNA.

4.6 RH1 in mTeSR Differentiation Assay

Cell viability assays showed IL4 cytotoxic to embryonic stem cells at $\geq$ 333 μg/mL, but the effect on pluripotency at lower concentrations had not yet been determined. A short assay was performed by the addition of 50 μg/mL to mTeSR. 50 μg/mL was chosen as it is significantly lower than the cytotoxic value, and higher than the MIC for *E. coli*. The morphology of cells showed no overall effect of IL4 in the

5 days growth, and the expression of pluripotency transcription factors Oct-4 and Nanog were measured to determine minor effects. No effect was observed on the expression of Nanog, but a 22% increase in Oct-4 expression was observed. The expression of Oct-4 is rapidly downregulated upon differentiation, but upregulation of Oct-4 expression might also induce differentiation[102]. The low increase combined with an unaltered morphology suggests that short term exposure to 50 μg/mL IL4 has little to no effect on the pluripotency of embryonic stem cells.

4.7 T8 in mTeSR Differentiation Assay

T8 is a pluripotency reporter cell line that express EGFP under control of the Oct-4 promoter. The cells are normally grown under selection pressure of G418, selecting only Oct-4 expressing cells, but small amounts of spontaneous differentiation was observed as soon as G418 was removed from the media. Six different media were prepared based on mTeSR. IL and IL4 were added to samples without bFGF and TGF-β to test for any positive effect of the peptides on pluripotency. mTeSR can support embryonic stem cells over extended periods, but the growth factors bFGF and TGF-β play important roles for proliferation and differentiation[103,104], and the removal of these will lead to significant differentiation within a few passages. The expression of EGFP by T8 cells was ment as an easy and noninvasive method to monitor pluripotency of human embryonic stem cells[23]. The T8 in mTeSR differentiation assay was performed in an attempt to develop a straight forward assay for screening of large libraries of compounds on hES cells.

The nuclear dye Hoechst stain was used to stain all cells. Hoechst stains DNA and all cells will bind the same amount of dye. The result of measurement of total fluorescence of each well during the first passage is shown in Figure 3.13. A high fluctuation of values combined with a significant autofluorescence made the approach unsuitable for a sensitive differentiation assay. Cell counting of EGFP positive cells was applied during the second passage. An EGFP/Hoechst ratio of 1 implies that all cells retain pluripotency, while a lowering of the value implies differentiation. Figure 3.15 shows the EGFP/Hoechst ratio during the second passage. The negative control drops to a minimum of 0.5 three days after passaging, but increases to 0.7 during the next two days. This development is not surprising as stem cells generally grow faster than differentiated cells. This also indicates that the used cell density of 3,125 cells/cm^2 at passaging puts the cells under a stress that especially the negative control is subjective to. The method of quantifying differentiation by counting of EGFP positive T8 cells proved to be a usefull approach, and a small increase of EGFP positive cells in samples added IL and IL4, compared to the reference, suggested that the peptides might have a positive effect on the preservation of pluripotency.

The assay was continued for two more passages. The morphology of the positive control remained ES like for the four passages, but the negative control spontaneously differentiated into two distinct mor-

phologies of which one consisted of elagonated mesoderm like cells. The sample added IL4 showed a high level of ES like cells, and real-time reverse-transcription PCR was performed to more precisely determine the effect on pluripotency. A positive effect of IL4 was evident, while IL had a negative effect on the maintenance of pluripotency. The expression of Nanog increased from passage two to passage four, which could not be explained, but Oct-4 expression correlated with the observed morphology. Only a single biological replicate was used for the assay and a replication of the experiment, confirming the result, would be required before any conclusion can be made of the effect of IL and IL4 on the preservation of pluripotency of embryonic stem cells.

A karyotype test was performed on the T8 cells, which showed that the cells used for the assay were aneuploidic before being subjected to treatment. The mutation of the cells was most likely the result of long time growth with G418. The test included 20 cells and also revealed a complex abnormal mosaic karyotype with the presence of three unbalanced cells lines. The cell line was most likely heterogeneous at the beginning of the assay and any results obtained could be a direct consequence of this.

4.8 RH1 in E8 Differentiation Assay

The E8 media is a simple media that consist of just eight components (including the DMEM/F12 base medium)[27]. The E8 media is simpler than the previously used mTeSR, and a gradual transition to E8 over 5 passages left the cells stressed as seen in Figure 3.18, where a large part of the cells were showing a flatter morphology than usual. The addition of 20 μg/mL IL had an immediate cytotoxic effect and 50μg/mL IL4 had a diminishing effect of the cell growth. These concentrations had no effect on the viability of cells in mTeSR, and the increase in toxic effect most likely comes from the cells being stressed and from the removal of BSA from the medium. mTeSR contains approximately 1% BSA (w/v), which could have a stabilising effect on the cell membrane. The peptide concentration was significantly lower than the required concentration for hemolytic activity and the exact cause of cell death could not be determined. It was however clear that the stressed embryonic stem cells had a significantly lower tolerance towards IL and IL4. The toxic effect of IL4 seemed to promote an unspecific differentiation as observed by the decrease in Nanog expression. The assay was not repeated with lower peptide concentrations due to the poor quality of the cells after the transition to E8 as seen from morphology and the drop in Nanog expression.

4.9 Investigating the DNA of HDF and RH1 cells

The difference in the epigenetic state of pluripotent stem cells and adult cells made the investigation of the DNA interesting, as chemical modifications of the nucleotides are unique to the state of the cells. The modifications in the chromatin are described in Section 1.2, and it is in particular the methylation and

hydroxymethylation of DNA that are of interest. Atomic force microscopy was chosen to investigate the binding of peptides to DNA, to test if the modifications of DNA had an effect on the binding affinity.

4.10 Fragmentation of DNA

Total DNA was isolated from the adult cells human dermal fibroblast (HDF) and from the embryonic stem cells Roslin Human 1 (RH1). Fragmentation of the DNA was desired as the length of the human chromosomes range from 48 to 249 million base pairs[105] and the distance between the base pairs is 3.4 Å[106] equaling a total length of 1.6 to 8.5 centimetre! The persistence length of duplex DNA is on the order of 500 Å[107], which means that a DNA chain larger than about 1,000 bp behaves like a flexible chain and will be coiled in solution. A high level of coiling is undesirable for AFM imaging and the fragmented DNA should not be larger than a few thousand base pairs.

4.10.1 Fragmentation by Sonication

Sonication of DNA was done using a Branson 2510. The apparatus is designed for ultrasonic cleaning, a process much more crude than the sensitive fragmentation of DNA molecules. The sonicater produces a frequency of 40kHz, which is in the range used for fragmentation of DNA[108,109]. Figure 3.22 and 3.24 shows that the sonication time required to obtain a certain level of fragmentation was higher for RH1 DNA than for HDF DNA, but a repeat of the experiment showed that the difference was a result of variation in sonication efficiency. The dimensions of the Branson 2510 water tank is 30 x 34 x 24 cm, and the positioning of the sample was of upmost importance as degradation of the DNA was only observed when the sample was placed in the center of short-lived standing waves.

The unfragmented DNA consisted of fragments sized between 30 and 100 kbp and not of chromosomal size. The large chromosomes were most likely ripped apart by shearing forces during pipetting and in particular fragmented by the use of a filter and centrifugation during the isolation process. The size distribution during the sonication process is shown in Figure 3.23 and 3.25. Background fluorescence, gel impurities and varying amount of DNA loaded in the wells make it hard to interpret the data, but a bell curved distribution is evident at increasing sonication times and espically in the RH1 DNA. The width of the distribution decreases as the DNA is fragmented and a Gaussian like distribution is obtained at prolonged sonication time, as seen in Figure 3.26. The degradation of DNA by sonication is belived to be a non-random process resulting in the preferential halving of the DNA molecules in solution[110], but a small preference for cleavage of d(CpG) has also been reported[109]. The obtained size distribution showed no sign of any preferential cleavage, and a uniform degradation of the entire DNA was achieved.

4.10.2 Restriction Enzyme Digestion of DNA

The restriction enzymes EcoRI and XhoI both have a recognition site length of 6 base pairs. Both enzymes should therefore statistically cleave once every 4,096 bp. The obtained size distribution was 750 bp to larger than 10,000 bp, and performing the digestion again had no effect on the size suggesting that a complete digestion had been performed.

4.11 High-resolution Atomic Force Microscopy

DNA isolated from HDF and from RH1 cells was successfully attached to APTMS-mica surfaces and imaged using atomic force microscopy. DNA molecules of several thousand nanometer length formed bundles on the surface and were unsuitable for investigation of the binding affinity of peptides. Aggregates of short strands (>100 nm) were observed in the HDF sample (Figure 3.28), but not in the RH1 sample (Figure 4.3). The entangled structure of the aggregates match the description by Limanskii *et al.* of single-stranded RNA molecules forming condensed multichain structures[111]. The HDF sample was treated with RNase A (Invitrogen) and gel electrophoresis (Figure 4.3) showed that the previously observed nucleic acids, smaller than the genomic DNA, was RNA. The multichain structures were not observed in AFM topography after treatment with RNase A. An incomplete treatment with RNase during cell isolation was probably the cause of RNA only showing in the HDF sample.

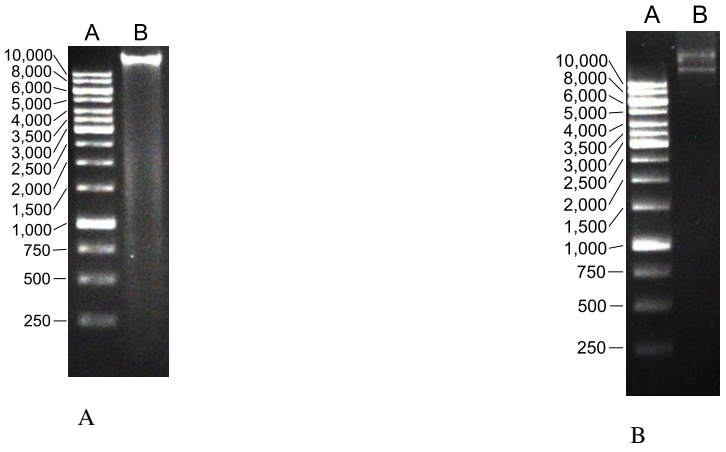

Figure 4.3: *Gel electrophoresis of HDF DNA, before (A) and after (B) treatment with RNase A. 1% agarose gels. RNA with a size distribution of 250 to 10,000 bp is clearly seen to be digested.*

DNA fragmented by sonication was imaged using AFM and the correlation to the size observed on gel was investigated. 3 minutes sonication of RH1 DNA yielded a distribution on gel with a mean migration length at 1,800 bp and a maximum concentration of 1,300 bp. The plotted mean however did not take into account the logarithmic correlation between DNA size and migration length[112]. The DNA ladder points are marked on the x-axis in Figure 3.25, and the DNA size as function of migration length obeys the exponential equation $f(x) = ae^{bx}$. The constants were fitted using MATLAB and the mean of the

DNA size distribution was calculated as 2,781 kbp for 3 minutes sonication and 2,643 kbp for 8 minutes sonication. It is essential to remember that a weighted mean is being used, as the fluorescence measured from the gel is proportional to the amount of base pairs. The mean size in a distribution composed of a single DNA piece of 1 kbp and 100 DNA pieces of 10 bp is 505 bp using the weighted mean, but only 19.8 bp when the arithmetic mean is calculated. The arithmetic mean can be determined from the DNA size distribution as

$$\sum \frac{f(x) * i}{\sum \frac{i}{f(x)}}, \tag{4.1}$$

where $f(x)$ is the DNA size corresponding to the migration length from the well and i is the color intensity at said size. The arithmetic mean DNA size after 3 minutes sonication of RH1 DNA was 1,966 bp and after 8 minutes 1,334 bp.

DNA is mainly in B-form when attached to a mica surface[113], and the axial rise of B-DNA is 0.34 nm / base pair. The mean DNA size observed with AFM was 280 nm for 3 minutes sonication and 245 nm for 8 minutes sonication (Figure 3.32) equal to 824 and 732 bp respectively. The DNA sizes observed with AFM were smaller than the corresponding gel electrophoresis results, and only few long DNA fragments were observed. The main reason for this result is most likely the formation of aggregations by long DNA strands, and degradation due to shear stress during the washing step before AFM imaging.

The average height of the fragmented DNA was only 6 to 8 Å, smaller than the theoretical diameter of 20 Å for B-DNA or the width of the minor groove of 12 Å[114]. Liu *et al* reported that DNA is mainly in B-form when attached to a mica surface functionalised by an amine, and they measured a height of 0.54 nm $\pm$ 0.07[113]. The decrease in size compared to dissolved DNA is most likely the result of force applied by the tip and attractive capillary forces mediated by the thin water layer that will always be adsorbed from the gas phase[115].

DNA fragmented by restriction endonuclease digestion contained a considerable amount of "dirt". EtOH precipitation was performed to remove protein, sugar and salt added during the digestion, but a complete removal of all contaminants could not be performed. Enzyme digestion is, unlike fragmentation by sonication, highly sequence dependent. DNA contain areas of repetitive sequences, and the goal of the fragmentation was to include the entire DNA, so fragmentation by sonication was preferred.

4.11.1 Binding of IL4 to DNA

The linearised pUC19 plasmid was used to determine the proper concentration of peptide that should be added to the DNA. A peptide concentration of 10 µg/mL was below the cytotoxic concentration mea-

sured on RH1 embryonic stem cells and corresponded to 4 - 10 mol peptide per mol base pair DNA. The negative charge of DNA phosphate groups and positive charge of IL4 should provide a rapid electrostatic binding, and the excess of IL4 will ensure coverage of all binding sites. The average height of pUC19 DNA was 6 - 8 Å, and the height increased to 10 - 12 Å when IL4 was added. The 0.4 nm increase in height clearly confirmed the binding of IL4 to the pUC19 plamid. A higher concentration of IL4 led to the formation of aggregates and was avoided.

A height increase of approximately 0.4 nm was observed when IL4 was added to HDF or RH1 DNA. To determine the difference in binding affinity of IL4 to the two DNA would require the analysis of a statistically significant amount of DNA. Hydroxymethylation of cytosine is a modification almost unique to embryonic stem cells. Approximately 4% of all cytosine species in CpG dinucleotides are hydroxymethylated[39], which means that the modification can be found in 1 of every 2000 base pairs. A 1µm x 1µm AFM scan of DNA fragmented by sonication normally yielded a total of 1 µm DNA correponding to approximately 3000 base pairs. IL4 showed a general affinity for DNA, and any effect of a hydroxymethylated cytosine would not be visible, but the combined method of fragmentation and AFM imaging holds the capacity of screening a sufficiently large amount of DNA to also include the special DNA base.

5 Conclusion

The effect of the peptides indolicidin and indolicidin-4 on human embryonic stem cells and in particular the interaction with their DNA has been investigated. The peptide IL4 was synthesised and the fluorophore rhodamine WT coupled at the N-terminus, creating the novel peptide IL4-RWT. Both peptides were purified by RP-HPLC and succesful synthesis confirmed by MS.

The cytotoxic concentrations of IL, IL4 and IL4-RWT on the hES cell lines RH1 and T8 were determined by growth of the cells on Matrigel^{TM} in mTESR®1. The cell uptake of the peptides was tested using the new peptide IL4-RWT by a combined method of high resolution microscopy and flow cytometry. A slow linear uptake indicated an endocytosis related pathway and a uniform intracellular distribution of the peptide was observed.

The effect of 50 μg/mL IL4 on pluripotency was tested on RH1 cells, and analysis of morphology and the expression of pluripotency transcription factors Oct-4 and Nanog showed that the peptide had no sifnificant effect over a short period. A long term assay was devised using the expression of EGFP by T8 cells, and the effect of 50 μg/mL IL4 or 20 μg/mL IL on pluripotency was tested. A clear positive effect of IL4 on the preservation of pluripotency was observed from EGFP expression, morphology and Oct-4 expression. Later karyotype testing of the T8 cells revealed a complex mosaic karyotype that was present before the cells were subjected to treatment. The mutation most likely yielded a heterogeneous cell population at the beginning of the assay making the results invalid. An increased toxic effect of IL and IL4 was observed when RH1 cells were transitioned to the chemically defined E8 media. The cells were stressed due to the transition, and it was observed that the tolerance of hES cells toward IL and IL4 is highly dependent on the cell condition and the media composition.

The binding of IL4 to hES cell DNA was investigated using AFM. DNA was isolated from HDF and RH1 cells and fragmented to enable attachment of separated DNA strands on a mica-APTMS surface for AFM imaging. Fragmentation was performed using ultrasonication and enzymatic digestion, of which ultrasonication was preferable as it produced proper sizes with no contaminations. Binding of IL4 to both HDF and RH1 DNA was confirmed by a height increase in AFM topographies of 0.4 nm. No difference was observed between the DNA of different sources, presumably due to the general affinity of IL4 to DNA, and due to the low frequency of modifications to the stem cell DNA. The combined method of fragmentation by sonication, attachment to a mica-APTMS surface and AFM imaging presented a fast method for visualisation and analysis of the DNA molecules.

References 6

[1] S. Ehnert, M. Glanemann, A. Schmitt, S. Vogt, N. Shanny, N. Nussler, U. Stöckle, and A. Nussler, "The possible use of stem cells in regenerative medicine: dream or reality?," *Langenbeck's Archives of Surgery*, vol. 394, no. 6, pp. 985–997, 2009.

[2] S. Sell, *Stem cells handbook*. Humana Pr Inc, 2004.

[3] E. Copelan, "Hematopoietic stem-cell transplantation," *New England Journal of Medicine*, vol. 354, no. 17, pp. 1813–1826, 2006.

[4] R. Lanza, *Handbook of stem cells*, vol. 2. Academic Press, 2004.

[5] U. D. o. H. National Institutes of Health and H. Services, *Stem Cell Information*. URL: `http://stemcells.nih.gov/info`, 2012.

[6] H. Zhou, S. Wu, J. Joo, S. Zhu, D. Han, T. Lin, S. Trauger, G. Bien, S. Yao, Y. Zhu, *et al.*, "Generation of induced pluripotent stem cells using recombinant proteins," *Cell stem cell*, vol. 4, no. 5, p. 381, 2010.

[7] M. Selsted, M. Novotny, W. Morris, Y. Tang, W. Smith, and J. Cullor, "Indolicidin, a novel bactericidal tridecapeptide amide from neutrophils.," *Journal of Biological Chemistry*, vol. 267, no. 7, pp. 4292–4295, 1992.

[8] C. Subbalakshmi and N. Sitaram, "Mechanism of antimicrobial action of indolicidin," *FEMS microbiology letters*, vol. 160, no. 1, pp. 91–96, 1998.

[9] C. Hsu, C. Chen, M. Jou, A. Lee, Y. Lin, Y. Yu, W. Huang, and S. Wu, "Structural and DNA-binding studies on the bovine antimicrobial peptide, indolicidin: evidence for multiple conformations involved in binding to membranes and DNA," *Nucleic acids research*, vol. 33, no. 13, p. 4053, 2005.

[10] Y. Nan, J. Bang, and S. Shin, "Design of novel indolicidin-derived antimicrobial peptides with enhanced cell specificity and potent anti-inflammatory activity," *Peptides*, vol. 30, no. 5, pp. 832–838, 2009.

[11] C. Marchand, K. Krajewski, H. Lee, S. Antony, A. Johnson, R. Amin, P. Roller, M. Kvaratskhelia, and Y. Pommier, "Covalent binding of the natural antimicrobial peptide indolicidin to dna abasic sites," *Nucleic acids research*, vol. 34, no. 18, pp. 5157–5165, 2006.

[12] Y. Nan, K. Park, Y. Park, Y. Jeon, Y. Kim, I. Park, K. Hahm, and S. Shin, "Investigating the effects of positive charge and hydrophobicity on the cell selectivity, mechanism of action and anti-inflammatory activity of a trp-rich antimicrobial peptide indolicidin," *FEMS microbiology letters*, vol. 292, no. 1, pp. 134–140, 2009.

[13] C. Friedrich, D. Moyles, T. Beveridge, and R. Hancock, "Antibacterial action of structurally diverse cationic peptides on gram-positive bacteria," *Antimicrobial agents and chemotherapy*,

vol. 44, no. 8, pp. 2086–2092, 2000.

[14] A. Ruzov, Y. Tsenkina, A. Serio, T. Dudnakova, J. Fletcher, Y. Bai, T. Chebotareva, S. Pells, Z. Hannoun, G. Sullivan, *et al.*, "Lineage-specific distribution of high levels of genomic 5-hydroxymethylcytosine in mammalian development," *Cell research*, vol. 21, no. 9, pp. 1332–1342, 2011.

[15] R. Dudek and J. Fix, *Embryology*. Lippincott Williams & Wilkins, 2005.

[16] J. Thomson, J. Itskovitz-Eldor, S. Shapiro, M. Waknitz, J. Swiergiel, V. Marshall, and J. Jones, "Embryonic stem cell lines derived from human blastocysts," *science*, vol. 282, no. 5391, p. 1145, 1998.

[17] J. Fletcher, P. Ferrier, J. Gardner, L. Harkness, S. Dhanjal, P. Serhal, J. Harper, J. Delhanty, D. Brownstein, Y. Prasad, J. Lebkowski, R. Mandalam, I. Wilmut, and P. Sousa, "Variations in humanized and defined culture conditions supporting derivation of new human embryonic stem cell lines," *Cloning and stem cells*, vol. 8, no. 4, pp. 319–334, 2006.

[18] C. Harley, H. Vaziri, C. Counter, R. Allsopp, *et al.*, "The telomere hypothesis of cellular aging.," *Experimental gerontology*, vol. 27, no. 4, p. 375, 1992.

[19] J. Nichols, B. Zevnik, K. Anastassiadis, H. Niwa, D. Klewe-Nebenius, I. Chambers, H. Scholer, and A. Smith, "Formation of pluripotent stem cells in the mammalian embryo depends on the pou transcription factor oct4," *Cell*, vol. 95, no. 3, pp. 379–391, 1998.

[20] J. Yu, M. Vodyanik, K. Smuga-Otto, J. Antosiewicz-Bourget, J. Frane, S. Tian, J. Nie, G. Jonsdottir, V. Ruotti, R. Stewart, *et al.*, "Induced pluripotent stem cell lines derived from human somatic cells," *Science*, vol. 318, no. 5858, p. 1917, 2007.

[21] K. Takahashi, K. Tanabe, M. Ohnuki, M. Narita, T. Ichisaka, K. Tomoda, and S. Yamanaka, "Induction of pluripotent stem cells from adult human fibroblasts by defined factors," *cell*, vol. 131, no. 5, pp. 861–872, 2007.

[22] N. Sato, I. Sanjuan, M. Heke, M. Uchida, F. Naef, and A. Brivanlou, "Molecular signature of human embryonic stem cells and its comparison with the mouse," *Developmental biology*, vol. 260, no. 2, pp. 404–413, 2003.

[23] L. Gerrard, D. Zhao, A. Clark, and W. Cui, "Stably transfected human embryonic stem cell clones express oct4-specific green fluorescent protein and maintain self-renewal and pluripotency," *Stem Cells*, vol. 23, no. 1, pp. 124–133, 2005.

[24] D. Hay, L. Sutherland, J. Clark, and T. Burdon, "Oct-4 knockdown induces similar patterns of endoderm and trophoblast differentiation markers in human and mouse embryonic stem cells," *Stem cells*, vol. 22, no. 2, pp. 225–235, 2004.

[25] T. Ludwig, M. Levenstein, J. Jones, W. Berggren, E. Mitchen, J. Frane, L. Crandall, C. Daigh, K. Conard, M. Piekarczyk, *et al.*, "Derivation of human embryonic stem cells in defined conditions," *Nature biotechnology*, vol. 24, no. 2, pp. 185–187, 2006.

[26] M. Martin, A. Muotri, F. Gage, and A. Varki, "Human embryonic stem cells express an immunogenic nonhuman sialic acid," *Nature medicine*, vol. 11, no. 2, pp. 228–232, 2005.

[27] G. Chen, D. Gulbranson, Z. Hou, J. Bolin, V. Ruotti, M. Probasco, K. Smuga-Otto, S. Howden, N. Diol, N. Propson, *et al.*, "Chemically defined conditions for human ipsc derivation and culture," *Nature methods*, vol. 8, no. 5, pp. 424–429, 2011.

[28] V. Akopian, P. Andrews, S. Beil, N. Benvenisty, J. Brehm, M. Christie, A. Ford, V. Fox, P. Gokhale, L. Healy, *et al.*, "Comparison of defined culture systems for feeder cell free propagation of human embryonic stem cells," *In Vitro Cellular & Developmental Biology-Animal*, vol. 46, no. 3, pp. 247–258, 2010.

[29] C. Hughes, L. Postovit, and G. Lajoie, "Matrigel: a complex protein mixture required for optimal growth of cell culture," *Proteomics*, vol. 10, no. 9, pp. 1886–1890, 2010.

[30] E. Jablonka, M. Lachmann, and M. Lamb, "Evidence, mechanisms and models for the inheritance of acquired characters," *Journal of Theoretical Biology*, vol. 158, no. 2, pp. 245–268, 1992.

[31] P. Collas, "Epigenetic states in stem cells," *Biochimica et Biophysica Acta (BBA)-General Subjects*, vol. 1790, no. 9, pp. 900–905, 2009.

[32] A. Bird *et al.*, "Cpg-rich islands and the function of dna methylation.," *Nature*, vol. 321, no. 6067, p. 209, 1986.

[33] G. Altun, J. Loring, and L. Laurent, "Dna methylation in embryonic stem cells," *Journal of cellular biochemistry*, vol. 109, no. 1, pp. 1–6, 2010.

[34] M. Bibikova, E. Chudin, B. Wu, L. Zhou, E. Garcia, Y. Liu, S. Shin, T. Plaia, J. Auerbach, D. Arking, *et al.*, "Human embryonic stem cells have a unique epigenetic signature," *Genome research*, vol. 16, no. 9, pp. 1075–1083, 2006.

[35] J. Deng, R. Shoemaker, B. Xie, A. Gore, E. LeProust, J. Antosiewicz-Bourget, D. Egli, N. Maherali, I. Park, J. Yu, *et al.*, "Targeted bisulfite sequencing reveals changes in dna methylation associated with nuclear reprogramming," *Nature biotechnology*, vol. 27, no. 4, pp. 353–360, 2009.

[36] R. Lister, M. Pelizzola, R. Dowen, R. Hawkins, G. Hon, J. Tonti-Filippini, J. Nery, L. Lee, Z. Ye, Q. Ngo, *et al.*, "Human dna methylomes at base resolution show widespread epigenomic differences," *nature*, vol. 462, no. 7271, pp. 315–322, 2009.

[37] G. Wyatt and S. Cohen, "The bases of the nucleic acids of some bacterial and animal viruses: the occurrence of 5-hydroxymethylcytosine," *Biochemical Journal*, vol. 55, no. 5, p. 774, 1953.

[38] N. Penn, R. Suwalski, C. O'Riley, K. Bojanowski, and R. Yura, "The presence of 5-hydroxymethylcytosine in animal deoxyribonucleic acid," *Biochemical Journal*, vol. 126, no. 4, p. 781, 1972.

[39] M. Tahiliani, K. Koh, Y. Shen, W. Pastor, H. Bandukwala, Y. Brudno, S. Agarwal, L. Iyer, D. Liu, L. Aravind, *et al.*, "Conversion of 5-methylcytosine to 5-hydroxymethylcytosine in mammalian dna by mll partner tet1," *Science*, vol. 324, no. 5929, pp. 930–935, 2009.

[40] S. Kriaucionis and N. Heintz, "The nuclear dna base 5-hydroxymethylcytosine is present in purkinje neurons and the brain," *Science*, vol. 324, no. 5929, pp. 929–930, 2009.

[41] R. Warren, "Modified bases in bacteriophage dnas," *Annual Reviews in Microbiology*, vol. 34, no. 1, pp. 137–158, 1980.

[42] S. Ito, A. D'Alessio, O. Taranova, K. Hong, L. Sowers, and Y. Zhang, "Role of tet proteins in 5mc to 5hmc conversion, es-cell self-renewal and inner cell mass specification," *Nature*, vol. 466, no. 7310, pp. 1129–1133, 2010.

[43] M. Zasloff, "Antimicrobial peptides of multicellular organisms," *Nature*, vol. 415, no. 6870, pp. 389–395, 2002.

[44] R. Hancock, "Cationic peptides: effectors in innate immunity and novel antimicrobials," *The Lancet infectious diseases*, vol. 1, no. 3, pp. 156–164, 2001.

[45] H. Boman, "Peptide antibiotics and their role in innate immunity," *Annual review of immunology*, vol. 13, no. 1, pp. 61–92, 1995.

[46] A. Rozek, C. Friedrich, and R. Hancock, "Structure of the bovine antimicrobial peptide indolicidin bound to dodecylphosphocholine and sodium dodecyl sulfate micelles.," *Biochemistry*, vol. 39, no. 51, p. 15765, 2000.

[47] P. Nicolas, "Multifunctional host defense peptides: Intracellular-targeting antimicrobial peptides," *FEBS Journal*, vol. 276, no. 22, pp. 6483–6496, 2009.

[48] W. Robinson, B. McDougall, D. Tran, and M. Selsted, "Anti-HIV-1 activity of indolicidin, an antimicrobial peptide from neutrophils," *Journal of leukocyte biology*, vol. 63, no. 1, p. 94, 1998.

[49] R. Halevy, A. Rozek, S. Kolusheva, R. Hancock, and R. Jelinek, "Membrane binding and permeation by indolicidin analogs studied by a biomimetic lipid/polydiacetylene vesicle assay," *Peptides*, vol. 24, no. 11, pp. 1753–1761, 2003.

[50] C. Subbalakshmi, E. Bikshapathy, N. Sitaram, and R. Nagaraj, "Antibacterial and hemolytic activities of single tryptophan analogs of indolicidin," *Biochemical and Biophysical Research Communications*, vol. 274, no. 3, pp. 714–716, 2000.

[51] Z. Oren and Y. Shai, "Mode of Action of Linear Amphipathic a-Helical Antimicrobial Peptides," *Biopolymers (Peptide Science)*, vol. 47, p. 451–463, 1998.

[52] M. Wu, E. Maier, R. Benz, and R. Hancock, "Mechanism of Interaction of Different Classes of Cationic Antimicrobial Peptides with Planar Bilayers and with the Cytoplasmic Membrane of Escherichia coli†," *Biochemistry*, vol. 38, no. 22, pp. 7235–7242, 1999.

[53] H. Schluesener, S. Radermacher, A. Melms, and S. Jung, "Leukocytic antimicrobial peptides kill autoimmune t cells," *Journal of neuroimmunology*, vol. 47, no. 2, pp. 199–202, 1993.

[54] P. Staubitz, A. Peschel, W. Nieuwenhuizen, M. Otto, F. Götz, G. Jung, and R. Jack, "Structure–function relationships in the tryptophan-rich, antimicrobial peptide indolicidin," *Journal of Peptide Science*, vol. 7, no. 10, pp. 552–564, 2001.

[55] H. Sader, K. Fedler, R. Rennie, S. Stevens, and R. Jones, "Omiganan pentahydrochloride (mbi 226), a topical 12-amino-acid cationic peptide: spectrum of antimicrobial activity and measurements of bactericidal activity," *Antimicrobial agents and chemotherapy*, vol. 48, no. 8, pp. 3112–3118, 2004.

[56] U. N. I. o. H. ClinicalTrials.gov, *Study of Antimicrobial Activity of Omiganan 1% Gel vs. Chlorhexidine 2% for Topical Skin Antisepsis in Healthy Adult Subjects*. URL: `http://`

clinicaltrials.gov/ct2/show/NCT00608959, 2008.

[57] C. Subbalakshmi, V. Krishnakumari, R. Nagaraj, and N. Sitaram, "Requirements for antibacterial and hemolytic activities in the bovine neutrophil derived 13-residue peptide indolicidin," *FEBS letters*, vol. 395, no. 1, pp. 48–52, 1996.

[58] P. Braga and D. Ricci, *Atomic force microscopy: biomedical methods and applications*, vol. 242. Humana Pr Inc, 2004.

[59] J. N. Israelachvily, *Intermolecular and Surface Forces*. No. ISBN: 0123751810, Academic Press Limited, 1992.

[60] L. Stiel and G. Thodos, "Lennard-jones force constants predicted from critical properties.," *Journal of Chemical and Engineering Data*, vol. 7, no. 2, pp. 234–236, 1962.

[61] Y. Martin, C. Williams, and H. Wickramasinghe, "Atomic force microscope-force mapping and profiling on a sub 100-å scale," *Journal of Applied Physics*, vol. 61, no. 10, pp. 4723–4729, 1987.

[62] Q. Zhong, D. Inniss, K. Kjoller, and V. Elings, "Fractured polymer/silica fiber surface studied by tapping mode atomic force microscopy," *Surface Science Letters*, vol. 290, no. 1-2, pp. L688–L692, 1993.

[63] J. Watson and F. Crick, "Molecular structure of nucleic acids," *Nature*, vol. 171, no. 4356, pp. 737–738, 1953.

[64] R. Dickerson, H. Drew, B. Conner, R. Wing, A. Fratini, and M. Kopka, "The anatomy of a-, b-, and z-dna," *Science*, vol. 216, no. 4545, pp. 475–485, 1982.

[65] J. van de Sande, N. Ramsing, M. Germann, W. Elhorst, B. Kalisch, E. von Kitzing, R. Pon, R. Clegg, and T. Jovin, "Parallel stranded dna," *Science*, vol. 241, no. 4865, pp. 551–557, 1988.

[66] A. Constantinou, A. Davies, and S. West, "Branch migration and holliday junction resolution catalyzed by activities from mammalian cells," *Cell*, vol. 104, no. 2, pp. 259–268, 2001.

[67] E. Raiber, R. Kranaster, E. Lam, M. Nikan, and S. Balasubramanian, "A non-canonical dna structure is a binding motif for the transcription factor sp1 in vitro," *Nucleic Acids Research*, vol. 40, no. 4, pp. 1499–1508, 2012.

[68] R. Sinden, *DNA structure and function*. Academic Pr, 1994.

[69] P. Russel, "igenetics: A molecular approach. 3 uppl," 2010.

[70] R. Peters, "Introduction to nucleocytoplasmic transport," *Xenopus protocols: cell biology and signal transduction*, vol. 322, p. 235, 2006.

[71] S. Anderson, A. Bankier, B. Barrell, M. De Bruijn, A. Coulson, J. Drouin, I. Eperon, D. Nierlich, B. Roe, F. Sanger, *et al.*, "Sequence and organization of the human mitochondrial genome," *Nature*, vol. 290, pp. 457–465, 1981.

[72] G. Elgar and T. Vavouri, "Tuning in to the signals: noncoding sequence conservation in vertebrate genomes," *Trends in Genetics*, vol. 24, no. 7, pp. 344–352, 2008.

[73] M. Cudic and J. Otvos, "Intracellular targets of antibacterial peptides," *Current Drug Targets*, vol. 3, no. 2, pp. 101–106, 2002.

[74] N. Knudsen, C. Poulsen, D. Le, C. Hansen, and L. Klausen, *Biophysical studies of interactions*

between indolicidin-4 and DNA in vitro and in silico. Aalborg University, 2009.

[75] J. Leppard and J. Champoux, "Human dna topoisomerase i: relaxation, roles, and damage control," *Chromosoma*, vol. 114, no. 2, pp. 75–85, 2005.

[76] J. Lhomme, J. Constant, and M. Demeunynck, "Abasic dna structure, reactivity, and recognition," *Biopolymers*, vol. 52, no. 2, pp. 65–83, 1999.

[77] D. Billingsley, W. Bonass, N. Crampton, J. Kirkham, and N. Thomson, "Single-molecule studies of dna transcription using atomic force microscopy," *Physical Biology*, vol. 9, p. 021001, 2012.

[78] S. Kasas, N. Thomson, B. Smith, P. Hansma, J. Miklossy, and H. Hansma, "Biological applications of the afm: from single molecules to organs," *International journal of imaging systems and technology*, vol. 8, no. 2, pp. 151–161, 1997.

[79] B. Wolf and S. Hanlon, "Structural transitions of deoxyribonucleic acid in aqueous electrolyte solutions. ii. role of hydration," *Biochemistry*, vol. 14, no. 8, pp. 1661–1670, 1975.

[80] E. Kay, "Double-stranded dna in methanol-ethanol-buffer solvent system," *Biochemistry*, vol. 15, no. 24, pp. 5241–5246, 1976.

[81] N. Thomson, S. Kasas, B. Smith, H. Hansma, and P. Hansma, "Reversible binding of dna to mica for afm imaging," *Langmuir*, vol. 12, no. 24, pp. 5905–5908, 1996.

[82] W. Chan and P. White, *Fmoc solid phase peptide synthesis: a practical approach*, vol. 222. Oxford University Press, USA, 2000.

[83] E. Kaiser, R. Colescott, C. Bossinger, P. Cook, *et al.*, "Color test for detection of free terminal amino groups in the solid-phase synthesis of peptides.," *Analytical biochemistry*, vol. 34, no. 2, p. 595, 1970.

[84] T. Christensen, "A chloroanil color test for monitoring coupling completeness in solid phase peptide synthesis," *Peptides–Structure and Biological Function*, vol. 85, 1979.

[85] M. Strohalm, M. Hassman, B. Košata, and M. Kodíček, "mmass data miner: an open source alternative for mass spectrometric data analysis," *Rapid Communications in Mass Spectrometry*, vol. 22, no. 6, pp. 905–908, 2008.

[86] M. Strohalm, D. Kavan, P. Nova´k, M. Volny´, and V. Havli´c?ek, "mmass 3: a cross-platform software environment for precise analysis of mass spectrometric data," *Analytical Chemistry*, vol. 82, no. 11, pp. 4648–4651, 2010.

[87] P. Corporation, *CellTiter-Blue™ Cell Viability Assay*. URL: `http://www.promega.com/~/media/Files/Resources/Protocols/Technical%20Bulletins/101/CellTiter-Blue%20Cell%20Viability%20Assay%20Protocol.pdf`, 2009.

[88] I. Horcas, R. Fernandez, J. Gomez-Rodriguez, J. Colchero, J. Gomez-Herrero, and A. Baro, "WSXM: A software for scanning probe microscopy and a tool for nanotechnology," *Review of Scientific Instruments*, vol. 78, p. 013705, 2007.

[89] D. Vasudevan, R. Fimmen, and A. Francisco, "Tracer-grade rhodamine wt: Structure of constituent isomers and their sorption behavior," *Environmental science & technology*, vol. 35, no. 20, pp. 4089–4096, 2001.

[90] S. Peri, H. Steen, and A. Pandey, "Gpmaw–a software tool for analyzing proteins and peptides," *Trends in biochemical sciences*, vol. 26, no. 11, pp. 687–689, 2001.

[91] J. Walker, *The protein protocols handbook*. Humana Pr Inc, 1996.

[92] D. Tai and R. Rathbun, "Photolysts of rhodamine-wt dye," *Chemosphere*, vol. 17, no. 3, pp. 559–573, 1988.

[93] D. P. A. D. Sousa, *Pluripotent Cell Translation*. URL: `http://www.crm.ed.ac.uk/research/group/pluripotent-cell-translation`, 2012.

[94] Y. Babaie, R. Herwig, B. Greber, T. Brink, W. Wruck, D. Groth, H. Lehrach, T. Burdon, and J. Adjaye, "Analysis of oct4-dependent transcriptional networks regulating self-renewal and pluripotency in human embryonic stem cells," *Stem Cells*, vol. 25, no. 2, pp. 500–510, 2007.

[95] T. Zwaka and J. Thomson, "Homologous recombination in human embryonic stem cells," *Nature biotechnology*, vol. 21, no. 3, pp. 319–321, 2003.

[96] K. Watanabe, M. Ueno, D. Kamiya, A. Nishiyama, M. Matsumura, T. Wataya, J. Takahashi, S. Nishikawa, S. Nishikawa, K. Muguruma, *et al.*, "A rock inhibitor permits survival of dissociated human embryonic stem cells," *Nature biotechnology*, vol. 25, no. 6, pp. 681–686, 2007.

[97] T. Falla, D. Karunaratne, and R. Hancock, "Mode of action of the antimicrobial peptide indolicidin," *Journal of Biological Chemistry*, vol. 271, no. 32, p. 19298, 1996.

[98] J. Richard, K. Melikov, E. Vives, C. Ramos, B. Verbeure, M. Gait, L. Chernomordik, and B. Lebleu, "Cell-penetrating peptides," *Journal of Biological Chemistry*, vol. 278, no. 1, p. 585, 2003.

[99] H. Yukawa, H. Noguchi, I. Nakase, Y. Miyamoto, K. Oishi, N. Hamajima, S. Futaki, and S. Hayashi, "Transduction of cell-penetrating peptides into induced pluripotent stem cells," *Cell Transplantation, 19*, vol. 6, no. 7, pp. 901–909, 2010.

[100] Y. Lin, S. Yao, R. Veach, T. Torgerson, and J. Hawiger, "Inhibition of nuclear translocation of transcription factor nf-κb by a synthetic peptide containing a cell membrane-permeable motif and nuclear localization sequence," *Journal of Biological Chemistry*, vol. 270, no. 24, pp. 14255–14258, 1995.

[101] L. Zhang, T. Torgerson, X. Liu, S. Timmons, A. Colosia, J. Hawiger, and J. Tam, "Preparation of functionally active cell-permeable peptides by single-step ligation of two peptide modules," *Proceedings of the National Academy of Sciences*, vol. 95, no. 16, p. 9184, 1998.

[102] H. Niwa, J. Miyazaki, A. Smith, *et al.*, "Quantitative expression of oct-3/4 defines differentiation, dedifferentiation or self-renewal of es cells," *Nature genetics*, vol. 24, no. 4, pp. 372–376, 2000.

[103] R. Xu, R. Peck, D. Li, X. Feng, T. Ludwig, and J. Thomson, "Basic fgf and suppression of bmp signaling sustain undifferentiated proliferation of human es cells," *Nature Methods*, vol. 2, no. 3, pp. 185–190, 2005.

[104] B. Greber, H. Lehrach, and J. Adjaye, "Fibroblast growth factor 2 modulates transforming growth factor β signaling in mouse embryonic fibroblasts and human escs (hescs) to support hesc self-renewal," *Stem Cells*, vol. 25, no. 2, pp. 455–464, 2007.

[105] G. R. Consortium, *Human Genome Assembly Information*. URL: http://www.ncbi.nlm.nih.gov/projects/genome/assembly/grc/human/data/index.shtml, 2012.

[106] B. Alberts, D. Bray, J. Lewis, M. Raff, K. Roberts, and J. Watson, "Molecular biology of the cell garland publishing," *New York*, pp. 3–11, 1994.

[107] G. Manning, "A procedure for extracting persistence lengths from light-scattering data on intermediate molecular weight dna," *Biopolymers*, vol. 20, no. 8, pp. 1751–1755, 1981.

[108] H. Elsner and E. Lindblad, "Ultrasonic degradation of dna," *DNA*, vol. 8, no. 10, pp. 697–701, 1989.

[109] S. Grokhovsky, I. Il'Icheva, D. Nechipurenko, M. Golovkin, L. Panchenko, R. Polozov, and Y. Nechipurenko, "Sequence-specific ultrasonic cleavage of dna," *Biophysical journal*, vol. 100, no. 1, pp. 117–125, 2011.

[110] D. Freifelder and P. Davison, "Studies on the sonic degradation of deoxyribonucleic acid," *Biophysical Journal*, vol. 2, no. 3, pp. 235–247, 1962.

[111] A. Limanskii, "Visualization of rna transcripts by atomic force microscopy," *Cytology and Genetics*, vol. 41, no. 2, pp. 76–81, 2007.

[112] J. Meyers, D. Sanchez, L. Elwell, and S. Falkow, "Simple agarose gel electrophoretic method for the identification and characterization of plasmid deoxyribonucleic acid.," *Journal of Bacteriology*, vol. 127, no. 3, pp. 1529–1537, 1976.

[113] Z. Liu, Z. Li, H. Zhou, G. Wei, Y. Song, and L. Wang, "Imaging dna molecules on mica surface by atomic force microscopy in air and in liquid," *Microscopy research and technique*, vol. 66, no. 4, pp. 179–185, 2005.

[114] R. Wing, H. Drew, T. Takano, C. Broka, S. Tanaka, K. Itakura, and R. Dickerson, "Crystal structure analysis of a complete turn of b-dna," *Nature*, vol. 287, pp. 755–758, 1980.

[115] A. Opitz, M. Scherge, S. Ahmed, and J. Schaefer, "A comparative investigation of thickness measurements of ultra-thin water films by scanning probe techniques," *Journal of applied physics*, vol. 101, p. 064310, 2007.

[116] M. Abràmoff, P. Magalhães, and S. Ram, "Image processing with imagej," *Biophotonics international*, vol. 11, no. 7, pp. 36–42, 2004.

Materials A

Material	Description	Manufacturer
Cell lines		
RH1	Roslin Human 1 human embryonic stem cell line	Roslin Institute
T8	Tranfected human embryonic stem clonal cell line	Roslin Institute
HDF	Human dermal fibroblast of neonatal foreskin origin	Royal I. Edinburgh
Chemicals		
APTMS	Lot# STBB4969V	Sigma Aldrich
Toluene 99.5%	Lot# 179418-1L	Sigma Aldrich
Ammonium Acetate 99.99%	Lot# MKBC8405	Sigma Aldrich
Dnase/RNase free water	Lot# MKBC8405	Sigma Aldrich
Agarose	Lot# A9539-500G	Sigma Aldrich
10X TAE buffer	Lot# 15558042	Invitrogen
Purelink Rnase A	Cat# 1044649	Invitrogen
Cell Titer Blue	G808A	Promega
Indolicidin	SP2275B	Cambridge Bioscience
mTeSR1	Cat# 05850	Stemcell technologies
5x Supplement	Cat# 05850	Stemcell technologies
rhTGFβ	Cat# 240-B	R&D Systems
mTeSR 5X supplement without Select Factors	Cat# 05892	Stemcell technologies
Matrigel	Cat# 354277	BD Biosciences
Trypsin/EDTA	Cat# 15090	Invitrogen
PBS	Cat# 10010	Invitrogen
TRIzol Reagent	Cat# 15596	Invitrogen
Low Serum Growth Supplement (LSGS)	S-003-10	Invitrogen
EcoRI	Cat# ER0271	Thermo Scientific
XhoI	Cat# ER0691	Thermo Scientific
Tango Buffer	Cat# BY5	Thermo Scientific
50 bp Generuler ladder	Cat# SM0373	Fermentas
1 kbp Generuler ladder	Cat# SM0313	Fermentas
Other		
AFM cantilever	Model: OMCL AC200TSE3, Lot# 911311	Atomic Force FE GmbH
Filter unit, 0.2 µm	Lot# 16532	Sartorius Stedim Biotech
Reaction Tubes	Lot: 616 201	Greiner bio-one
Muscovite mica	Lot# 71856-01	Electron Microscopy S. Inc.
24 well culture dish	3524	Corning Incorporated
96 Well Cell Culture Microplates	Cat# 655090	Greiner Bio-one
SuperScript III First-Strand	Cat# 18080-051	Invitrogen
DyNAmo Flash SYBR Green qPCR	F-415	New England Biolabs
DNeasy Blood n Tissue Kit	69504	Qiagen

Matrigel stock solution

10 mL Matrigel was thawed on ice, mixed with 10 mL 4 °C Knockout DMEM, 1 mL aliquoted to each of 15 mL falcons and stored at -20 °C. The aliquot was thawed on ice when needed, added 14 mL 4°C Knockout DMEM, mixed and stored for up to 7 days at 4 °C.

Collagenase solution

10 mg collagenase type IV in Knockout DMEM (Invitrogen). Filter sterilised and stored at -20 °C.

0.025% Trypsin/EDTA solution

250 mL PBS was added 2.5 mL 2.5% Trypsin (Invitrogen) and 150 µL 0.5 M EDTA disodium. Filter sterilised and stored at -20 °C.

Cell Viability Assay B

Cytotoxicity of the peptides IL, IL4 and IL4-RWT was tested on the embryonic stem cell lines RH1 and T8 using the CellTiter-Blue^{TM} Cell Viability Assay[87]. Relative cell viability values were obtained from each well of a 96 well plate as:

$$\frac{F_S - F_E}{F_R - F_E} \tag{B.1}$$

F_S is the fluorescence measured from the sample testing the effect of a specific peptide concentration, F_E is fluorescence measured from wells added no cells at the beginning of the assay, but fed the same peptide concentration and F_R is the fluorescence measured from the reference consisting of cells growing without addition of peptide. All fluorescence values were obtained using 560 nm excitation and 590 nm emission.

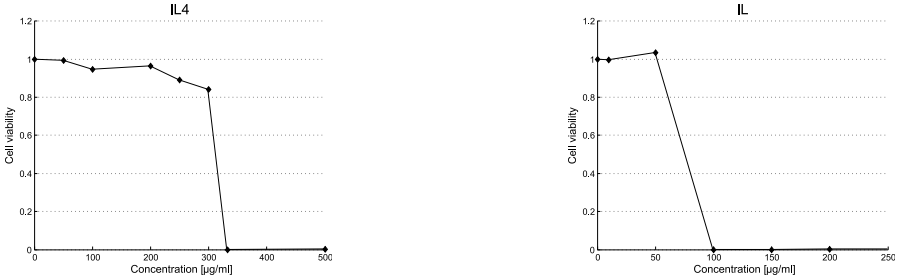

A B

Figure B.1: *Relative cell viability of RH1 cells after growth on media added increasing concentrations of IL4 (A) or IL (B). Each point is the mean of a triplicet.*

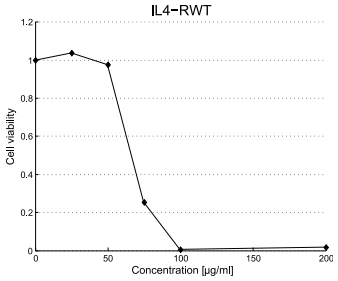

Figure B.2: *Relative cell viability of RH1 cells after growth on media added increasing concentrations of IL4-RWT. Each point is the mean of a triplicet.*

C Quantification of EGFP Positive T8 Cells

Quantification of eGFP Positive T8 Cells was done by staining with the fluorescent Hoechst stain. Hoechst stain is a cell permeable day that becomes blue fluorescent upon binding to DNA. Figure C.1 shows the green and blue fluorescence of T8 cells after Hoechst staining.

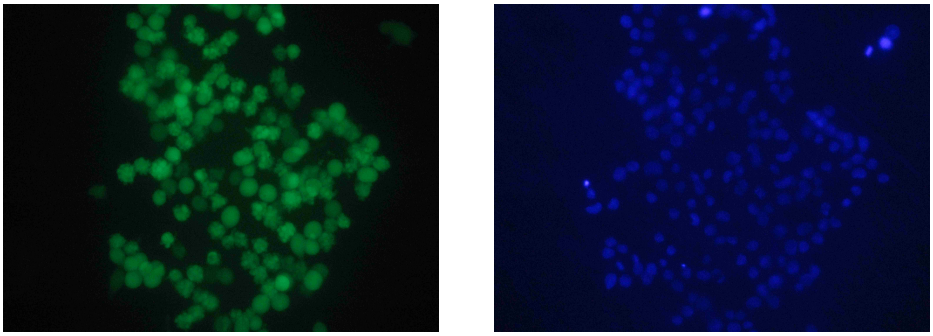

A B

Figure C.1: *Hoechst and EGFP flourescence from T8 cells.*

Cell counting was done using the image processing program ImageJ[116] and a self-made script. Steps of the image analysis can be seen in Figure C.2.

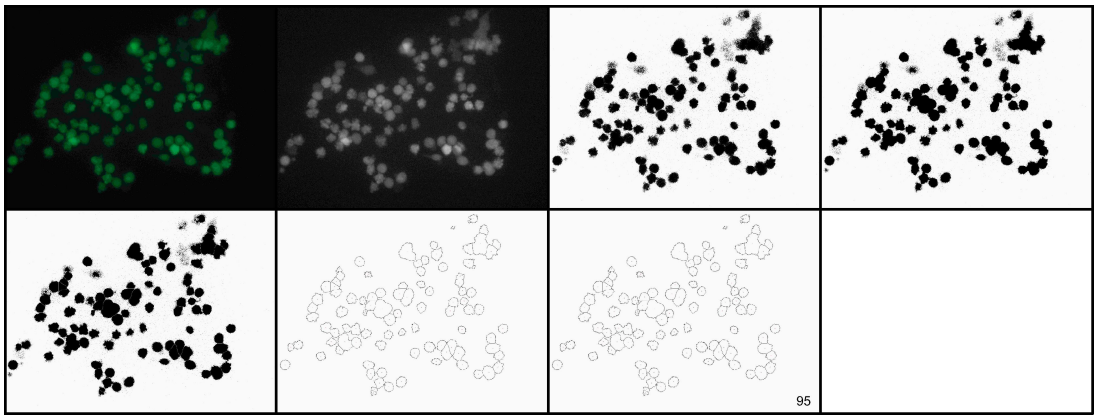

Figure C.2: *Automated cell counting procedure in ImageJ.*

The process of cell counting was only accurate until 5 days from passaging as the fluorescent signal of cells were overlapping when the cell density became too high.

D Real-Time Reverse-Transcription PCR

Total RNA was isolated from a minimum of 1 million cells. The purity of reverse transcribed cDNA was examined by PCR using GAPDH primers and the Biotaq^{TM} Red DNA Polymerase kit (Bioline) to ensure that no genomic DNA was carried over. Figure D.1 shows gel electrophoresis of samples with genomic DNA contamination. Two samples were prepared for reverse transcription and the superscript enzyme replaced with water in one of them. The pairs of sample and negative control were loaded in the gel in pairs.

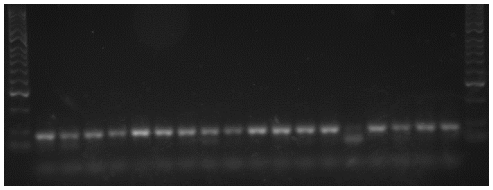

Figure D.1: *2% gel electrophoresis of isolated RNA to test for DNA contamination. Reverse transcription of the same samples with and without enzyme are loaded in pairs.*

Figure D.2 shows gel electrophoresis of the same samples after RQ1 RNase-Free DNase (Promega). No amplification was observed showing that the sample was free of (mammalian) DNA.

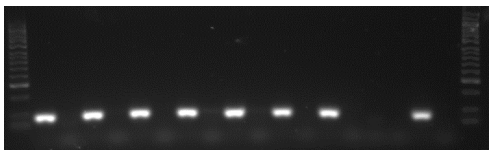

Figure D.2: *2% gel electrophoresis of isolated RNA to test for DNA contamination. Reverse transcription of the same samples with and without enzyme are loaded in pairs.*

mRNA transcription levels were analysed using the StepOne software v2.1 (Applied Biosystems). A comparative C_T method was applied with an automatically set threshold cycle by the machine. An amplification plot obtained in the project is shown in Figure D.3.

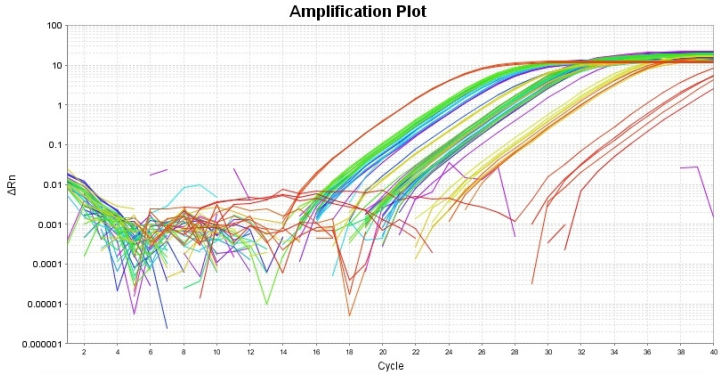

Figure D.3: *Amplification plot.*

The fluorescence increases for each cycle as the amount of double stranded DNA increases. Auto fluorescence and fluorescence from unspecific DNA dominates during the first 14-18 cycles until the exponential amplification of the target DNA dominates and the amount of double stranded DNA is doubled every cycle. The cycle at which the fluorescence exceeds a certain threshold, C_t, is used to estimate the amount of the gene, and this threshold cycle is automatically set by the software based on background fluorescence from the negative controls (added only water). The amount of the target gene is normalised to the amount of GAPDH in the same sample to take into account the difference in amount of starting RNA. The reported "fold difference" is calculated as:

$$\frac{X_{sample}}{X_{reference}} = 2^{\Delta\Delta C_T} = 2^{\left(C_{T,sample} - C_{T,GAPDH}\right)_{reference} - \left(C_{T,sample} - C_{T,GAPDH}\right)_{sample}} \tag{D.1}$$